

## Keery et al., Sensitivity of the Eocene Climate to CO<sub>2</sub> and Orbital Variability

### Responses to Reviewers

We have amended the manuscript to address the issues raised by the reviewers. We have included comments on the limitations and advantages of models of intermediate complexity in the Methods and Summary sections. We have expanded our discussion of the responses of the monsoons, including the American monsoon, to orbital cycle, and clarified comparisons of our results with temperature proxy measurements.

Details are provided below in our responses to each of the two reviewers, with reviewers' comments in black, and our responses in red.

In addition to our responses to the reviewers' comments, we have recalculated main effects and total effects without using an approximation in the calculation of variances, resulting in only very minor numerical differences, and no change to our main findings. We have prepared amended versions of Table 4 and Figures 10 and 11, and made very minor changes to the text, where appropriate.

We have included calculations of climate sensitivity for a doubling of atmospheric CO<sub>2</sub>, added a new figure to illustrate this, and amended the Results section to include our findings with respect to a dependency of climate sensitivity on low or high states of CO<sub>2</sub> concentration:

Figure 7 shows the relationship between CO<sub>2</sub> (plotted on a logarithmic scale), and MAT, with an abrupt change of gradient clearly visible at a CO<sub>2</sub> concentration of 1000 ppm. From the two gradients, we derive climate sensitivity values for a doubling of CO<sub>2</sub> concentration at CO<sub>2</sub> levels below 1000 ppm, and at CO<sub>2</sub> levels above 1000 ppm, of 4.36°C and 2.54°C respectively. We note that our modelled values of carbon in vegetation in the ENTS module remain low outside of the tropics at low CO<sub>2</sub> concentration, but as CO<sub>2</sub> concentration increases, land areas at higher latitudes reach maximum values of carbon in vegetation, with all land areas showing no further capacity for increased carbon in vegetation at an atmospheric concentration of ~1000 ppm. The increase in land vegetation cover, with corresponding reduction in albedo, acts as a positive feedback to rising temperature caused by increasing CO<sub>2</sub>, but this feedback mechanism ceases to operate when all available land is at its maximum vegetation capacity, with a consequent reduction in the climate sensitivity.

and we have included the following text in the Summary:

Our modelling results suggest that climate sensitivity is state dependent, with a value of 4.36°C in a low CO<sub>2</sub> state, and 2.54°C in a high CO<sub>2</sub> state, due to a positive feedback mechanism in which albedo reduces as vegetation increases to its maximum value when CO<sub>2</sub> concentration reaches 1000 ppm.

Responses to each of the reviewers, and the amended manuscript with markup, are included below.

## Keery et al., Sensitivity of the Eocene Climate to CO<sub>2</sub> and Orbital Variability

Response to M. Crucifix (Referee)

Referee comments in black

Author responses in red

We are very grateful for this thorough review.

### 1 Summary

Keery et al. present a sensitivity analysis of the Eocene climate to four factors: CO<sub>2</sub> concentration, eccentricity, obliquity, and precession angle. They use, to this end, the PLASIM-GENIE model (details in their section 3) with suitable palaeogeography. The methodology relies on a 50-member hyper-cube sample of a 5-d space (one extra dummy variable was added), and linear modelling with a Information Criteria for model selection. Experiment output are summarised using fit-for-purpose summaries like “tropical-polar temperature difference” and monsoon indices, as well as principal components obtained from a singular value decomposition. The authors conclude on the importance of CO<sub>2</sub> for global mean temperature, and of the orbital elements for the spatial distribution and regional weather systems such as monsoons.

### 2 Main comments

1. The paper is in the line of a number of recent studies attempting to estimate the relative sensitivity of the climate system to CO<sub>2</sub> and orbital forcing, using a methodology founded on ensemble of experiments. This includes, in addition to the Holden et al. (2015) and Bounceur et al. (2015) cited, Araya-Melo et al. (2015) and Lord et al. (2017). Keery et al. is the only article to focus on the Eocene, which makes it an original contribution. It also uses a much simpler methodology than Araya-Melo et al. (2015), Bounceur et al. (2015), and Lord et al. (2017) because it uses linear regression instead of a Gaussian process emulator. In fact, the authors reference to the word “emulator” is slightly unusual because emulation is, in the climate literature, often used to designate statistical meta-modelling with a focus on uncertainty quantification. Claiming (p. 8) that a “similar emulator approach has been applied by Bounceur et al. 2015” is therefore somewhat misleading. Bounceur et al. and Araya-Melo et al. applied the developments of Oakley and O’Hagan (2004) with, in the case of Bounceur, the additional complication of the PCA emulator.

We agree that the comparison of our emulator to the emulators developed by Araya-Melo et al. (2015) and Bounceur et al. (2015) was misleading, and we have amended this section:

Our emulator approach uses linear regression, rather than a Gaussian process (GP), and is therefore simpler than the methods applied by Bounceur et al. (2015) in a study of the response of the climate-vegetation system in interglacial conditions to astronomical forcing, and by Araya-Melo et al. (2015) in their study of the Indian monsoon in the Pleistocene.

In spite of its simplicity, we are confident that our approach may be correctly described as an emulator, as it fulfills the criteria described by O’Hagan (2006), and cited by Araya-Melo et al. (2015):

- it is derived from a small number of model runs filling the entire multidimensional input space
- once the emulator is built, it is not necessary to perform any additional runs with the model

In passing, Araya-Melo et Lord used HadCM3 which shows that ensemble-based sensitivity analysis to orbital forcing is doable with GCMs (this qualifies the author’s comment on line 15, p.2).

We have amended this paragraph to acknowledge recent ensemble studies using GCMs:

Climate simulations with high temporal and spatial resolution can be obtained from General Circulation Models (GCMs), but the requirement of GCMs for powerful computers and long run-times makes them difficult to deploy for large ensembles of model simulations and restricts their ability to investigate the large uncertainties in forcings and model parameterisations. Such ensembles are more practical with more heavily parameterised and hence more computationally efficient Earth system Models of Intermediate Complexity (EMICs), (Weber, 2010), although we note that Araya-Melo et al. (2015) and Lord et al. (2017) have deployed the GCM HadCM3 in ensemble-based studies of orbital forcing effects on climates of the Pleistocene and late Pliocene respectively.

Of course, the fact that other authors have adopted a more sophisticated methodology invalidates by no means the approach used by Keery et al.: there may be no need to use a sledgehammer to crack a nut. It remains that the methodological set up used here is a step backwards compared to recent studies, and this arguably requires some justification. How much do we lose with the linearity assumption, and which impact does it have on the uncertainties of the quantification of main effects? (see comment 3. more specifically on main effects).

As we have noted in our methods section, we have demonstrated that the linear models can be used to emulate PC scores with very high correlations to the PC scores derived directly through SVD, with examples from temperature and precipitation shown in Table 3. We can therefore be confident that main effects derived from the linear models are robust. We have amended the text:

Unlike linear models, GP models are intrinsically stochastic and give a more accurate quantification of their own error in emulating the input data. However, GP models can become computationally demanding in high dimensional space, and their results can be more difficult to interpret.

2. Experiment design. The authors do not say much about the ensemble design, except that this is a latin hypercube. There are many ways to do a latin hypercube, and it usually involves additional constraints.

We have added a detailed description of the method used to generate the latin hypercube in an appendix, include forcing factor values for the full ensemble in a new Table, and we have amended the main text:

The present study has been designed to facilitate direct comparison between the results for specific ensemble members and their direct counterparts in a future study using the EMIC model GENIE-1 (Edwards and Marsh, 2005), which will include additional forcing parameters not used by this PLASIM-GENIE study. We have applied an iterative method to generate a pair of corresponding hypercubes with five and eleven dimensions for the PLASIM-GENIE and GENIE-1 studies respectively, in which the minimum Euclidean distance between any two points is maximised, and linear correlation between any two parameters is minimised. Details of the steps taken to generate the hypercubes are provided in Appendix A. The absolute value of the r correlation coefficient does not exceed 0.1 for any pair of input (forcing and dummy) parameters. Uniform ranges for each of the forcing parameters and the dummy parameter are shown in Table 1, and the values applied in all 50 PLASIM-GENIE ensemble members are shown in Table 2.

In fact this experiment design raises some doubts. For example, why are some secondary structures (periodic up and downs) apparent in the response to obliquity, Figure 5, middle column? Is this just a subjective visual impression?

We have created an additional plot of the two forcing factors obliquity and CO<sub>2</sub>, for discussion, but not for inclusion in the paper, and this shows a very similar pattern to the obliquity-MAT subplot in Figure 5, with corresponding clusters and the same slight impression of periodicity. We can therefore be confident that the apparent periodicity noted by the reviewer in the model output is an artefact of randomly generated structure in the model input.

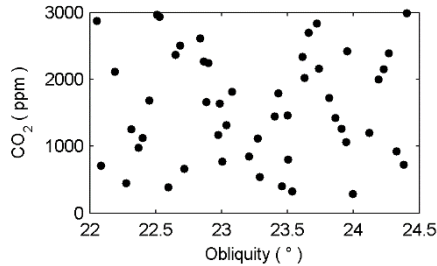


Figure R1 Obliquity plotted against CO<sub>2</sub>.

One potentially problematic element is the definition of the sampled astronomical space. It seems that latin hypercube sampling is made on axes along  $e$ ,  $\omega$  (longitude of perihelion) and  $\varepsilon$ . If this is what the authors have been doing then this is non-physical. We know that the astronomical forcing generates effects through seasonal and daily insolation, which are very well approximated by linear functions of  $e \sin \omega$  (which the authors call the precession index on Fig. 6) and  $e \cos \omega$ . This is the reason why several authors have chosen to sample the astronomical space following the axes  $e \sin \omega$  and  $e \cos \omega$  and regress against these components. Presumably the regression analysis by Keery is indeed done against these indices but the text is not always clear. Lines 1-2 p. 8. rather suggest that the explanatory variables were  $\sin \omega$  and  $\cos \omega$  (instead of their multiplication by  $e$ ) and the lines 4-5 p. 11 are quite confusing. Hopefully the choice of regression variables is mainly matter of text clarification, but the design of the latin hypercube may have a more fundamental problem.

We have indeed constructed our hypercube by sampling independently on  $e$ ,  $\omega$  (longitude of perihelion) and  $\varepsilon$ , but we do not agree that this is non-physical, as there are no combinations of these parameters which can be excluded for the early Eocene period. If we have ignored any information which would imply that some combinations are less likely to have occurred than others (we are not aware of any), then this would only result in a minor reduction in the efficiency with which we fill our state space. We note that precessional effects are well approximated by  $e \sin \omega$  and  $e \cos \omega$ , and that several authors have chosen to sample and regress against these components, but we have chosen not to take this approach, as it would not allow any climatic effects of eccentricity which may exist independently of precession to be identified. We have amended our description of the forcing factors:

In order to investigate the sensitivity of the Eocene climate to variation in atmospheric CO<sub>2</sub> and orbital parameters, we have constructed an ensemble of 50 model configurations, each with a unique set of forcing parameters comprising atmospheric CO<sub>2</sub>, eccentricity ( $e$ ), obliquity ( $\varepsilon$ ) and precession ( $\omega$ ), the angle on the Earth's orbit around the Sun between the moving vernal equinox and the longitude of perihelion (Berger et al., 1993). When  $e$  is zero, the Earth's distance from the Sun is constant at all points on the orbit, so there is no precessional effect. The magnitude of precessional effects is controlled by  $e$ , while phase is controlled by  $\omega$ , so precessional effects are commonly described by the precession index given by  $e \sin \omega$ . The only orbital parameter which alters the total annual solar radiation received by the Earth is  $e$ , although the range of variation is very small. We include  $e$  and  $\omega$  as separate and independent forcing parameters, rather than combined as the precession index, or in the form  $e \cos \omega$ . This approach does not make the assumption that the only effect of eccentricity on the Earth's climate is through its effect on the

amplitude of the precession cycle, but allows experimental results to be examined for effects of  $e$  and  $\omega$  either separately or in combination. An additional dummy parameter is included to test for possible overfitting of relationships between forcing parameters and model output fields.

We have also amended our description of our preparation of the forcing factors for linear modelling:

Values of the forcing parameters  $\text{CO}_2$ ,  $e$  and  $\varepsilon$  (with its very small angular range considered to be approximately linear) were normalised to the range  $[-1, 1]$  and combined with  $\sin\omega$  and  $\cos\omega$  to form 50-element column vectors representing the forcing factors.

3. There may be some confusion about the meaning of the main effects. Saltelli does not use the phrase “first order” to mean linear approximation. In a case where only one factor would matter (be the relationship linear or not), the main and total effects would match (Saltelli et al. (2004), ch. 1 states clearly the definitions; or refer again to Oakley and O’Hagan (2004)). More generally, computing main and total effects is not trivial and always involves some approximations. More details on their computation would be welcome.

We have amended the text to provide more details on the computation of the main effects and total effects:

In order to analyse the results of each of our linear models, we apply the method described in detail by Holden et al. (2015) to derive the main effects (Oakley and O’Hagan, 2004), which provide a measure of the variation in the linear model output due to each of the terms (first order, second order and cross products), derived from their coefficients, and total effects (Homma and Saltelli, 1996), which separate the effect of each forcing parameter on the variation in the model output. Although the forcing factors are all scaled within the range  $[-1, 1]$ , the trigonometrical precession terms are not uniformly distributed across this range. We have therefore computed the variances of the first order, second order and cross product terms directly for all parameters, rather than applying the respective approximations of  $\frac{1}{3}$ ,  $\frac{1}{9}$  and  $\frac{4}{45}$ , and we have applied these values as scaling factors in calculating the main effects and total effects.

4. Singular value decomposition is a great dimensionality reduction methodology, but how much is learned by analysing the behaviour of principal components separately is a more contentious subject. Identification of principal components can be fragile to some implementation details, such as, e.g. grid area weighting and experiment design, and the physical phenomena which give rise to climate variability need not be orthogonal. In fact physical modes may project poorly on the orthogonal vectors (Monahan and Fyfe, 2006). These caveats implicitly acknowledged by the authors (p. 11, ll. 20-21) but this state-of-affairs poses some questions about the emphasis on principal components in this article.

We have amended the text to acknowledge these caveats:

We perform a singular value decomposition to identify the PCs and empirical orthogonal functions (EOFs) of temperature and precipitation fields in the full ensemble, although we note that climate variability may not be due to physical processes which vary orthogonally, and identification of PCs can be influenced by aspects of the experimental design.

### 3 Minor (scientific) comments

- How Fig. 2 should be interpreted is not entirely clear since the ensemble was not explicitly designed so that the ensemble mean is an estimate of the Eocene climate mean.

Figures 2 and 4 are included to provide an illustrative summary of the spatial distribution and variation of temperature and precipitation in the full ensemble output, without implying that the ensemble mean is an estimate of the Eocene climate mean. We have amended the text:

Analysis of the model results has focused on variation in surface air temperature and precipitation in both winter and summer in each hemisphere, although it should be noted that our experiment has not been designed such that mean values in our ensemble output represent direct estimates of the Eocene climate mean.

#### 4 Minor (editorial) comments

- Introduce subtitle after section 2.

We have introduced the subtitle ‘Climate of the Early Eocene’

- Material about cyclostratigraphy under section 2.1.2. may possibly be considered for shortening as slightly out of scope of the article. This said this is an interesting read.

We would prefer to retain the section on cyclostratigraphy in full, as we believe it provides important details which are relevant to our experimental design, particularly our selection of independent orbital values, and the separation of  $e$  and  $\omega$ .

- PLASIM-GENIE does not need a specific section: it can fall under section 3.Methods.

This section has been moved to the Methods as suggested by both reviewers.

- p. 6 reference Gough (1981) is mistakenly repeated.

The duplicated reference has been removed.

- p. 7, the sentence “We apply the linear algebraic tool SVD” sounds unnecessarily sophisticated. Why not “We perform a singular value decomposition to identify principal components”

We have amended this sentence:

We perform a singular value decomposition to identify the PCs and empirical orthogonal functions (EOFs) of temperature and precipitation fields in the full ensemble.

- p. 10, l. 27 : define the word “precession” precisely.

We have made amendments to the text to define precession ( $\omega$ ), and the precession index ( $e\sin\omega$ ). See our response to an earlier comment.

- p. 12, ll. 13-17 : introducing new results so close to the closing words is usually not encouraged.

We have deleted these results, as further analysis suggests it is difficult to draw any very useful conclusions from the extra experiment, and we have amended the text to include the reference to Anagnostou et al. (2016):

If atmospheric CO<sub>2</sub> remained within a narrower range throughout the period, for example in the range 700 to 1800 ppm indicated for the early Eocene by Anagnostou et al. (2016) in a recent study using boron isotopes, then outside of short-lived hyperthermals, the relative influence of CO<sub>2</sub> and orbital inputs might have been more evenly balanced.

#### 5 Digital material

- Relevant data of the Eocene runs (at least the summaries and experiment input data) could be provided.

We have included the values of forcing factors for the 50 member ensemble in a new Table.

#### References

P. A. Araya-Melo, M. Crucifix, and N. Bounceur. Global sensitivity analysis of the indian monsoon during the pleistocene. *Climate of the Past*, 11:45–61, 2015. doi: 10.5194/cp-11-45-2015. URL <http://www.clim-past.net/11/45/2015/>.

N. Bounceur, M. Crucifix, and R. D. Wilkinson. Global sensitivity analysis of the climatevegetation system to astronomical forcing: an emulator-based approach. *Earth System Dynamics*, 6:205–224, 2015. doi: 10.5194/esd-6-205-2015. URL <http://www.earth-syst-dynam.net/6/205/2015/>.

- P. B. Holden, N. R. Edwards, P. H. Garthwaite, and R. D. Wilkinson. Emulation and interpretation of high-dimensional climate model outputs. *Journal of Applied Statistics*, pages 1–18, 2015. doi: 10.1080/02664763.2015.1016412. URL <http://dx.doi.org/10.1080/02664763.2015.1016412>.
- N. S. Lord, M. Crucifix, D. J. Lunt, M. C. Thorne, N. Bounceur, H. Dowsett, C. L. O’Brien, and A. Ridgwell. Emulation of long-term changes in global climate: Application to the late pliocene and future. *Climate of the Past Discussions*, page 1–47, 2017. ISSN 1814-9359. doi: 10.5194/cp-2017-57. URL <http://dx.doi.org/10.5194/cp-2017-57>.
- A. H. Monahan and J. C. Fyfe. On the nature of zonal jet eofs. *Journal of Climate*, 19: 6409–6424, 2006. ISSN 1520-0442. doi: 10.1175/jcli3960.1. URL <http://dx.doi.org/10.1175/JCLI3960.1>.
- J. E. Oakley and A. O’Hagan. Probabilistic sensitivity analysis of complex models: a bayesian approach. *Journal of the Royal Statistical Society: Series B (Statistical Methodology)*, 66: 751–769, 2004. doi: 10.1111/j.1467-9868.2004.05304.x.
- A. Saltelli, S. Tarentola, F. Campolongo and M. Ratto, *Sensitivity Analysis in Practice: A guide to assessing scientific methods* John Wiley and Sons Ltd., 219pp., 2004.

Referee comments in black

Author responses in red

We are very grateful for this thorough review.

This paper reports on an ensemble of 50 Eocene climate-model simulations, each of which characterized by a different combination of eccentricity, obliquity, precession and atmospheric CO<sub>2</sub> concentration. The climate model is the PLASIM-GENIE model, a new model of intermediate complexity, recently introduced by Holden et al. (2016). The study aims to summarize the ensemble of paleoclimate simulations by looking at what-they-call “simple metrics”, principal component analysis and an emulator approach. This study provides a couple of interesting results. The first is the existence of a seaice-related threshold mechanism in the northern hemispheric high latitudes. From Figure 2 and 3, it seems that when a certain threshold in the extent of DJF-sea-ice is exceeded, temperatures (both sea-surface and maritime air temperatures) drop significantly. It would be interesting to read the author’s opinion how this compares to the recent findings of modeling work by Zeebe et al. (2017), who found that “High-latitude mechanisms are unlikely drivers of orbitally paced changes in the late Paleocene-early Eocene”. The interesting role of (seasonal) sea-ice in the climate system of the early Eocene aspect remains, however, rather underdeveloped in the present version of the paper.

In our discussion of Figs. 2 & 3 [page 9, line 10] we have stated: "The variation in TPTD across the ensemble thus appears to be essentially driven by the strength of snow and ice albedo feedback", and a little further on, in our discussion of Fig. 5 [page 9, line 22], in particular the plot of CO<sub>2</sub> v northern winter TPTD we have declared: "and it can also be seen that CO<sub>2</sub> strongly affects the northern TPTD in the winter, but not in the summer, when the combined influence of obliquity and precession index is discernible, suggesting that temperature proxies with seasonal bias may have a significant orbital imprint. The plot of atmospheric CO<sub>2</sub> against N. Winter TPTD shows a change in gradient at approximately 1000 ppm CO<sub>2</sub> and 32°C. This may be related to the logarithmic dependence of radiative forcing on CO<sub>2</sub> concentration, as well as the disappearance of ice above some threshold level, cf Fig. 3."

We have added the additional comment:

A possible sea ice related threshold mechanism influencing both SST and maritime air temperature in high northern latitudes may be observed in Fig. 3, and this is strongly associated with the increase in northern winter TPTD at low CO<sub>2</sub> levels. Zeebe et al. (2017) have analysed a high resolution benthic isotope record covering the late Palaeocene - early Eocene, and have concluded that orbitally paced cycles are unlikely to have been driven by high latitude mechanisms, but our PLASIM-GENIE modelling suggests that while northern TPTD is not orbitally paced in the winter, being controlled by CO<sub>2</sub>, it is orbitally paced in the summer, by a combination of obliquity and precession.

The second interesting aspect is the distinct response to precession of monsoonal precipitation and temperature in the different monsoonal systems (e.g. Figure 6). The description and discussion of these Eocene paleoclimate simulations is useful and perfectly fits the scope of the journal. The current version of the manuscript is, however, unsatisfactory for publication in *Climate of the Past* for the reasons listed below.

## Major Comments

1. One of the major conclusions in the current version of the manuscript, is that 95The emulator approach adopted in this study allows for estimating the response of different aspects of the climate system (e.g. wet-season monsoonal precipitation) over the full input space. It would -for example- be interesting to see the response of precipitation and temperatures in the different monsoonal systems to astronomical forcing for specific pCO<sub>2</sub> levels. This could be an elegant way to circumvent the disparity in time-scales between CO<sub>2</sub> and orbital variability.

We have amended the subplots for obliquity and precession index in Figures 5 and 6 to denote the CO<sub>2</sub> level on a continuous colour scale. This approach gives a simple visual indication of which relationships between the astronomical forcing factors and the temperature and precipitation simple metrics are influenced by CO<sub>2</sub>. Figure 6 also now includes an additional row of subplots for the American monsoon index.

We have applied emulators derived from linear modelling of the forcing factors and monsoon indices, to estimate values of each of the monsoon indices over the full range of precession ( $\omega$ ), with fixed high eccentricity ( $e$ ), for low and high values of CO<sub>2</sub>, and low and high values of obliquity ( $\epsilon$ ).

We have made amendments to the abstract:

The results demonstrate the importance of orbital variation as an agent of change in climates of the past, and we demonstrate that emulators derived from our modelling output can be used as rapid and efficient surrogates of the full complexity model, to provide estimates of early Eocene climate conditions from any set of forcing parameters.

and to the final paragraph of the introduction:

By applying the linear modelling and emulation methods of Holden et al. (2015), we regress both the simple scalar metrics and the SVD reduced dimension model outputs onto the forcing parameters, and from the derived relationships, we infer main effects denoting the effect of each explanatory term in the linear model, and total effects denoting the effect of each forcing parameter, on the variation in the scalar metrics and on the temperature and precipitation output fields. We demonstrate that emulators derived in respect of tropical precipitation metrics can be used to estimate Eocene monsoonal responses to any combination of GHG and orbital forcing parameter values.

We have added new Figures 12, 13 and 14, plotting emulated values of the Asian, African and American monsoon indices.

We have added a paragraph to the Results section:

We apply the linear models derived from the forcing factors and monsoon indices as emulators to estimate values of monsoon indices corresponding to the full range of precession ( $\omega$ ), with eccentricity fixed at its high limit of 0.06, low and high values of CO<sub>2</sub> (300 ppm and 3000 ppm), and low and high values of obliquity (22.0° and 24.5°). Precession index ( $e\sin\omega$ ) and emulated values of the Asian, African and American monsoon indices are plotted in Figures 12, 13 and 14 respectively. Relationships between the precession index and the monsoon indices which are visually suggested in Figure 6 are shown with clear structure in Figures 12, 13 and 14. In each of the monsoon areas, the increase in precipitation due to precession effects is more pronounced at high atmospheric concentration of CO<sub>2</sub>, and also at high obliquity.

We have added a paragraph to the Summary;

We have demonstrated that emulators derived from linear modelling of the PLASIM-GENIE ensemble results can be used as a rapid and efficient method of estimating climate conditions from any set of forcing parameters, without the need for further deployment of the EMIC.

2. The authors do not provide their 50-simulation experimental design. It is essential to have an overview of the parameter settings for each simulation that was run in the framework of this study. The details on the settings of the 50 simulations could be given either in the form of a Table, or in the form of a figure, or in both forms. For good examples, please check Figure 2 and Table 1 in Araya-Melo et al. (2015, cp-11-45-2015), Figure 2 and Table 2 in Lord et al. (2017, cp-2017-57), and Figure 1 in Bounceur et al. (2015, esd-6-205-2015).

We have included the values of the forcing factors and the dummy variable for the ensemble in a new table (Table 2).

We note that Araya-Melo et al. (2015) constrained their experiment to exclude non-physical combinations of CO<sub>2</sub> and sea ice, and their Figure 2 includes an informative subplot showing fairly strong inverse correlation between CO<sub>2</sub> and sea ice. In our study, however, we do not have a priori information with which to constrain any combinations of our forcing factors, each of which is sampled independently to maximise state space coverage and to minimise correlations between the forcing factors. We include in this response a new figure showing cross-plots and  $r$  coefficients of all of the forcing factors and the dummy parameter, which illustrate both the coverage of the state space, and the very low correlation between any of the factors. We do not consider that this figure, or a variation, could add significant information to that included in the text, which has been amended to include the statement:

The absolute value of the correlation coefficient  $r$  does not exceed 0.1 for any pair of input (forcing and dummy) parameters.

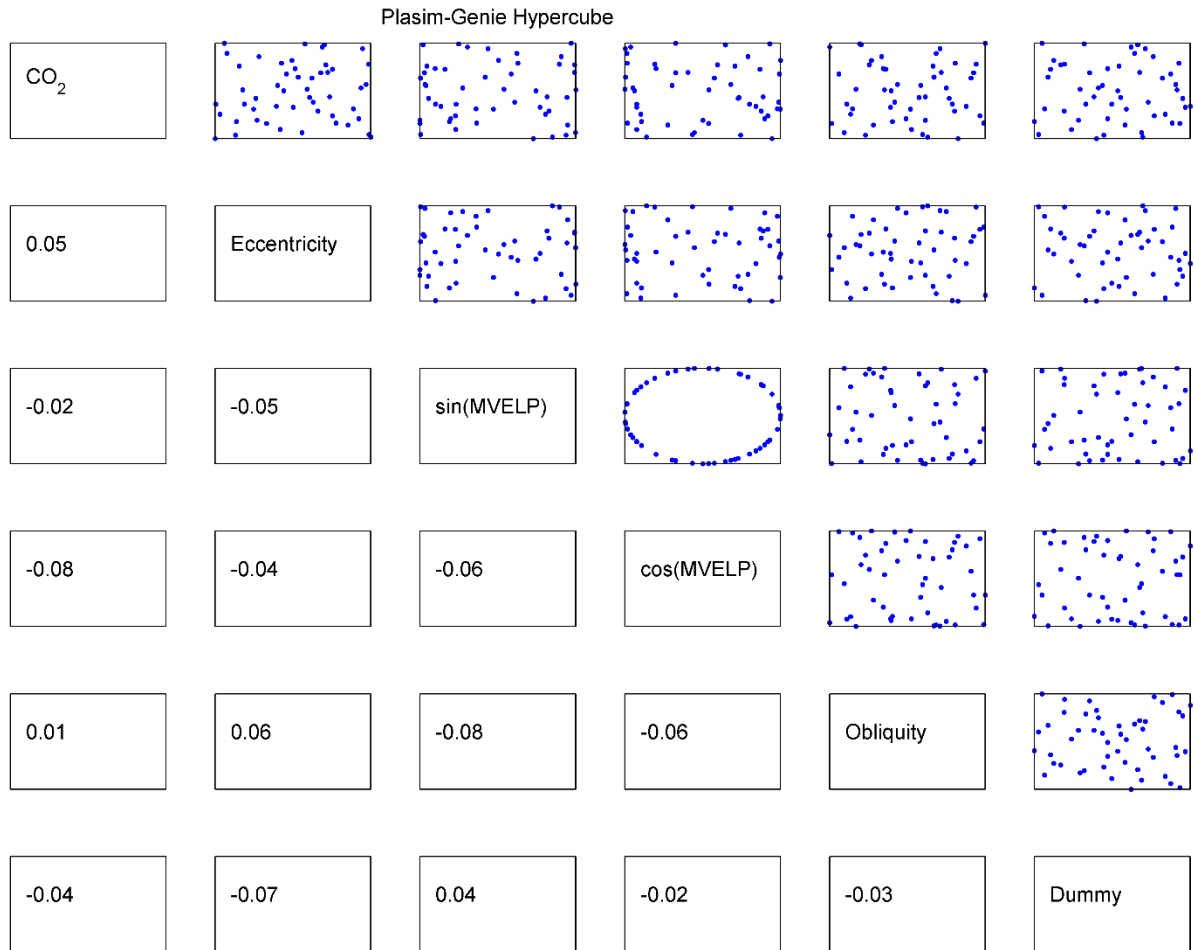


Figure R2 Correlation plots and  $r$  coefficients between all forcing factors.

3. From Figure 6, it is very clear that precession has an important influence on the Asian Monsoon intensity, with higher rainfall when the index is minimum (i.e. Earth in perihelion during JJA, maximum northern hemisphere summer insolation). However, if I interpret PC2 in JJA temperature and PC2 in JJA precipitation correctly (Table 5 and Figures 7 and 8), it seems that a precession-driven increase in monsoonal rainfall coincides with a decrease in JJA temperature in the Asian Monsoon region. Such a decrease in temperature is remarkable, given that it occurs when northern hemisphere JJA insolation is maximum. This observation can either be explained by the consumption of incoming solar radiation as latent heat, or by a negative influence of the increased cloud cover on the radiation balance. Indeed, the reflective character of clouds contributes to the planetary albedo. In the revised version of the manuscript, I would like to read more discussion of paleoclimate mechanisms like this one.

This temperature decrease is indeed observed in the model results for the Asian monsoon. We have augmented the text to describe this effect more clearly:

An increase in the second PC scores for JJA precipitation in the Asian monsoon region (Fig. 9) corresponds to a decrease in the second PC scores for JJA temperature (Fig. 8), and as already noted, the second PC scores for both temperature and precipitation in JJA are strongly correlated to the precession index. This temperature reduction during the Asian monsoon was also observed by Holden et al. (2014), and attributed to a reduction in incoming solar radiation associated with increased cloud cover and surface evaporation.

4. Page 7, lines 23-25 and Figure 6: When I was first interpreting Figure 6, I was confused by the fact that the Asian Monsoon and the African monsoon seemed to respond to precession in the same way, despite the fact that they are located on opposite sides of the equator. It took me quite a while to realize that both monsoonal systems are responding to precession in the expected way: with intensified wet-season precipitation in the Asian Monsoon system when the Earth reaches perihelion in JJA (negative precession index), and intensified wet-season precipitation in the African Monsoon system when the Earth reaches perihelion in DJF (positive precession index). I only understood this after reading lines 23-25 (page 7) several times. Indeed, the authors define their monsoon-related “simple scalar metric” by the difference in rainfall in DJF and JJA, regardless of whether DJF is the wet or the dry season in the monsoonal system considered. This also explains why the panel of Figure 6 that is related to the African Monsoon shows negative values, whereas the panel that is related to the Asian Monsoon exhibits positive values. I would strongly advise the authors to think about ways to illustrate the monsoonal response to precession in a more intuitive way. Maybe the paper by Tuenter et al (2003) could provide some inspiration as to how to best present the response of a summer monsoon to precessional (and obliquity?) forcing. Also, why is the South American monsoon system missing from Figure 6?

We have amended our monsoon indices so that each is now derived by subtracting winter precipitation from summer precipitation, as suggested. Figure 6 has been altered accordingly, and now also includes a row for the American monsoon index, an entry for which will be added to the table of total effects of forcing parameters on simple scalar metrics (presently Table 3; will be Table 4).

We have amended the text to reflect the changes to the monsoon indices:

In this study, we derive simple scalar metrics to denote indices for monsoons for Asia, Africa and South America by subtracting winter rainfall from summer rainfall, for defined geographical regions, denoted on Fig. 1, and selected for their similarity to monsoonal regions in the modern continental configuration.

We have amended our comments on Figures 5 and 6 in the Results section, following addition of the American monsoon index, and the use of colour in these Figures:

In Figs. 5 and 6,  $\text{CO}_2$ , obliquity ( $\varepsilon$ ) and precession index ( $\varepsilon \sin \omega$ ) are plotted against MAT, northern seasonality, northern winter TPTD and northern summer TPTD (Fig. 5), and southern winter polar OLC, northern winter polar OLC, Asian monsoon index, African monsoon index and American monsoon index (Fig. 6). Subplots for obliquity and precession index in Figures 5 and 6 denote the  $\text{CO}_2$  level on a continuous colour scale.

and we have added the comment:

The American monsoon index is fairly strongly correlated with the precession index at high levels of  $\text{CO}_2$ , and negatively correlated with  $\text{CO}_2$  at low levels of  $\text{CO}_2$ .

We note that the study by Tuenter et al. (2003) included six experimental setups, with each one comprising either maximum or minimum values of obliquity, and maximum, minimum or zero values of precession. They were therefore able to illustrate their results in the form of spatial patterns of the differences in output values for pairs of experiments with contrasting values of one or both forcing factors. This approach is not appropriate for our 50 member ensemble, with uncorrelated forcing factor values, in which no pairs of experiments can be identified for this type of comparison.

## Additional comments and recommendations

Abstract line 5 and p. 2 lines 1-3: I would recommend being a little bit more conservative on the possible analogy between the PETM and the ongoing anthropogenic disturbance of the global carbon cycle. Also cite Zeebe et al. (2016, Nature Geoscience) here.

We have amended the text to clarify the importance of the PETM, particularly its importance as the closest, if not perfect, analogue to anthropogenic climate change, and to include a citation of Zeebe et al (2016):

Since the PETM is the most recent period in Earth's history for which estimated atmospheric GHG concentrations are similar in magnitude to those of the present-day, and expected to arise from fossil fuel burning, the PETM may provide a valuable analogue for anthropogenic climate change (e.g. McInerney and Wing, 2011; Zeebe et al., 2016; Zeebe and Zachos, 2013).

Abstract: The abstract reads too technical and vague. I find the following sentence particularly vague: "Two dimensional model output fields are reduced to scalar values through simple summarizing algorithms and by singular value decomposition." The reader gets very little information from this sentence. I would recommend rewriting the abstract, making it more results-oriented.

We have deleted this sentence, and made amendments to the abstract to make it less vague, with more focus on the results, including our additional work on climate sensitivity, and using the emulators.

Page 2, line 30: suggestion: "The Earth resided in a greenhouse state"

We don't understand the reason behind this suggestion. Our intention was to emphasise that the greenhouse state had been continuous since the early Cretaceous, so we will leave the sentence unchanged.

Page 3, line 4: What do you mean with "high levels of radiative forcing"? Only eccentricity influences the total amount of solar energy received by the Earth: : but the amplitude of that variability is only 0.15

Huber & Caballero (2011) used CO<sub>2</sub> as a proxy for all changes to incoming and outgoing radiation. They commented "We have not addressed whether the enhanced radiative forcing was due to pCO<sub>2</sub>, methane, other greenhouse gases, novel cloud feedbacks, or other "missing" factors. We have also not established whether large forcing is actually necessary, the alternative being high values of climate sensitivity as in the study of Heinemann et al. (2009) and only moderate increases in forcing."

We have amended the text to clarify this:

Huber and Caballero (2011), hereafter HC11, have demonstrated that with sufficiently high levels of CO<sub>2</sub> (as a proxy for all forms of radiative forcing), climate models can generate global air temperature distributions in broad agreement with the proxy temperature measurements.

Page 2, line 9: Either you provide the reader with information on which kind of evidence exists. Or you rewrite like: "During the PETM, the emission of organic carbon was initially in the form of methane, which later oxidized to CO<sub>2</sub>".

We have amended the text to give brief details of the evidence, and we will include an additional citation:

There is some evidence from analysis and modelling of the timing and duration of variations in  $\delta^{13}\text{C}$  and  $\delta^{30}\text{S}$  observed in nannoplankton fossils that some of the GHG emissions were initially in the form of CH<sub>4</sub> (Dickens, 2011; Lunt et al., 2011; Thomas et al., 2002), which is rapidly oxidised in the atmosphere to CO<sub>2</sub>.

Page 2, line 23: "broadly similar" is quite a subjective, interpretative qualification. I find the Eocene paleogeography quite different from today's, given that the Tethys Ocean was still open. If you want to point to the similarity with the present-day, you could state that the majority of the continents were located in the northern hemisphere.

We have used the phrase “broadly similar” in the sense that the continental configuration is instantly recognisable, unlike for example, the Triassic period, with a single supercontinent just starting to break up into those that we’re familiar with today. We have amended this paragraph:

The arrangement of the continents and oceans in the Early Eocene was broadly similar to that of the present, with the Earth’s land mass divided into the same major continents, and with most of the land mass in the northern hemisphere. India had not yet collided with the Eurasian continent, and the closure of the Tethys Ocean was not yet complete. Such tectonic movements may have effected some changes to the climate system. In particular, the configuration of ocean gateways strongly influences modes of ocean circulation, and hence affects energy transport throughout the climate system (Lunt et al., 2016; Sijp et al., 2014).

Page 4, line 10 and many other occurrences: “dominant periods of 100 kyr and 405 kyr”. In an eccentricity power spectrum there are 4 peaks around 100 kyr, but only a single one at 405 kyr. Therefore, I would suggest the above notation.

We note that there are multiple peaks in the power spectra for eccentricity, equivalent to a single peak with a period of approximately 100 ka, together with an isolated peak for eccentricity with a period of 405 ka. There are similar clusters of peaks around 40 ka for obliquity, and around 20 ka for precession. We have amended the text to use the approximation symbol ‘~’ in respect of the obliquity, precession and 100 ka eccentricity cycles, but not in respect of the 405 ka eccentricity cycle:

The main oscillations are the eccentricity of the Earth’s orbit around the Sun, with periods of ~100 ka and 405 ka, the obliquity or tilt of the Earth’s axis of rotation, with a period of ~40 ka, and precession, the relative timing between perihelion and the seasons, with a period of ~20 ka (Berger et al., 1993).

Page 4, line 16: Jacques Laskar does not calculate time scales. He calculates astronomical solutions.

We have replaced “astronomical time scale” with “astronomical solution”.

Page 5: Why is Section 3 not a subsection of Section 4 “Methods”?

This section has been moved to the Methods as suggested by both reviewers.

Page 5, line 3: What is “T21”?

We have amended this sentence to clarify that T21 denotes the resolution obtained through spectral modelling:

We apply the model at a spectral T21 atmospheric resolution, which corresponds to a triangular truncation applied at wave number 21 and a horizontal resolution of  $5.625^\circ$ , with 10 layers, and a matching ocean grid with 32 depth levels.

Page 6, lines 9-11: An injection of carbon into the atmosphere is measured in tons of C, whereas the concentration of CO<sub>2</sub> in the atmosphere is measured in ppm. These are thus two different things, with two different units. You have to rephrase this sentence to correct for that.

We have amended the sentence as follows:

Although the maximum mass of CO<sub>2</sub> injected into the atmosphere during CIEs, and in particular the PETM, remains uncertain, there is broad agreement that the atmospheric concentration of CO<sub>2</sub> did not exceed 3000 ppm (e.g. Gehler et al., 2016), and that it did not fall below the pre-industrial level of 280 ppm at any time during the early Eocene.

Page 6, lines 13-16: It’s not immediately clear to me how knowledge on the phase relationship between carbon isotope excursions and the astronomical parameters would influence the experimental design of your study. If you would know these phase relationships, would you then have designed your experiments differently?

If these relationships were known, we would have been able to concentrate our investigation on combinations of the orbital forcing parameters of particular interest, i.e. those considered to be important in respect of the CIEs. We have amended this paragraph:

Since the absolute astronomical time scale for the early Eocene has an uncertainty which is greater than the periods of the obliquity and precession cycles, and there remains disagreement as to which phases of the eccentricity cycles are related to CIEs, there are no combinations of the orbital forcing parameters which can be known a priori to be of greater importance in their effects on the Eocene climate in general, and on their contributions to the initiation, duration and termination of the CIEs in particular. We therefore select values of orbital parameters independently, and from the full range of each parameter's variation during the early Eocene.

Page 6, line 26: What do you mean with “quasi-steady state”?

We have added the phrase "a spin-up period of" to clarify that the "quasi-steady" state is the state of approximate equilibration of the model after the model has run for long enough such that the initial conditions have been 'forgotten'.

Page 7, line 7-8: The atmospheric circulation patterns during the Eocene were most definitely different from those in the modern world. I think you can remove the “are likely to”.

We agree, and we have replaced “are likely to have differed” with “will have differed”.

Page 7 line 27: Spell out SVD

We have amended this sentence to accommodate suggestions from both reviewers:

We perform a singular value decomposition to identify the PCs and empirical orthogonal functions (EOFs) of temperature and precipitation fields in the full ensemble

Page 8 line 9: Please provide the appropriate references where these criteria are defined.

We have provided the appropriate references for the Akaike information criterion (Akaike, 1974), and Bayes information criterion (Schwarz, 1978), and since these are of a highly technical nature, we have added a reference to a much cited textbook on model selection:

Burnham and Anderson (2003) provide a detailed discussion of the application of information criteria in model selection.

Page 8 lines 23-24: The Figure 3 that you are referring to, only contains global annual mean SST's, not the Arctic winter SST's you are discussing.

We have amended the text:

We note that the Arctic winter median air temperature is below freezing over both land and sea in the PLASIM-GENIE ensemble, (see Fig 3) and the Arctic does not remain ice-free throughout the year in any of the 50 simulations in our study.

Page 9, line 1: It is unclear to me what exactly you mean with “parametric uncertainty”

We have amended the text for clarification:

Quantification of model-related uncertainty is beyond the scope of the present study.

Page 10, line 17: JJA instead of JJF.

We have corrected this error.

Page 10, line 15: Shouldn't this be Table 4?

We have corrected this error – it is now Table 5, following earlier insertion of an additional table.

The paper contains a few important shortcomings when it comes to appropriately referencing pre-existing work.

For example, the authors do not refer to the Deep-time Model Intercomparison Project (Deep-MIP, Lunt et al., 2017, gmd-10-889-2017). The authors do not frame their study within that project, nor do they differentiate their study from that project. A statement on this topic is indiscernible, given that both this study and the Deep-MIP project explicitly focus on simulating (early) Eocene warm climates and that both are using the same paleogeographic configuration from Herold et al. (2014).

This paper was at the final stages of preparation when Lunt et al. (2017) was published online (on 23 February 2017). We are pleased to note that their recommended palaeogeography is that of Herold et al. (2014) which we have used as the basis for the palaeogeography in our study. We have amended the first sentence in the description of our model configuration:

This study was designed before Lunt et al. (2017) presented their 'DeepMIP' guidelines for model simulations of the latest Paleocene and early Eocene. However, our palaeogeography is based on the high-resolution digital reconstruction of the early Eocene published by Herold et al. (2014), and which Lunt et al. (2017) recommended should be used as the standard for all palaeoclimate simulations within the DeepMIP framework. We have used the dataset of Herold et al. (2014) as an initial configuration for the tectonic layout, topography and bathymetric boundary conditions in our study.

We have also added a comment on the solar constant:

We note that Lunt et al. (2017) have recommended that a modern value of  $1361.0 \text{ W m}^{-2}$  should be applied to studies within the DeepMIP framework, in order to facilitate comparison between simulations with modern and pre-industrial levels of  $\text{CO}_2$ , and to offset the absence of elevated levels of  $\text{CH}_4$ .

The authors refer to Bounceur et al. (2015), who applied a “similar emulator approach” (p. 8 line 13). First of all, I am unsure whether that statement is technically correct. Secondly, this reference is missing from the reference list.

We have ensured that Bounceur et al. (2015) are included in the reference list, and we have amended the text to clarify our comparison with their approach:

Our emulator approach uses linear regression, rather than a Gaussian process (GP), and is therefore simpler than the methods applied by Bounceur et al. (2015) in a study of the response of the climate-vegetation system in interglacial conditions to astronomical forcing, and by Araya-Melo et al. (2015) in their study of the Indian monsoon in the Pleistocene.

On page 4, line 28, the authors give credit to Ruddiman (2006, cp-2-43-2006) for noting “a relationship between obliquity and the extent of northern ice sheets”. First of all, this is a Pleistocene-focused paper, of which I don't really see the relevance when discussing orbital configurations during the Eocene and possible influence on climate. Moreover, the relationship between obliquity-induced minima in NH summer insolation and ice age cycles was already suggested by Milutin Milankovitch in 1941.

We agree that this is misleading, and adds little to the paper. We have deleted it.

## References

- Bounceur, Nabila, Michel Crucifix, and R. D. Wilkinson. "Global sensitivity analysis of the climate-vegetation system to astronomical forcing: an emulator-based approach." *Earth System Dynamics* 6.1 (2015): 205.
- Herold, N., Buzan, J., Seton, M., Goldner, A., Green, J. A. M., Müller, R. D., Markwick, P., and Huber, M.: A suite of early Eocene (â Lij 55 Ma) climate model boundary conditions, *Geosci. Model Dev.*, 7, 2077–2090, doi:10.5194/gmd-7-2077-2014, 2014.
- Tuenter, Erik, et al. "The response of the African summer monsoon to remote and local forcing due to precession and obliquity." *Global and Planetary Change* 36.4 (2003): 219-235.
- Zeebe, Richard E., Andy Ridgwell, and James C. Zachos. "Anthropogenic carbon release rate unprecedented during the past 66 million years." *Nature Geoscience* 9.4 (2016): 325-329.
- Zeebe, R. E., T. Westerhold, K. Littler, and J. C. Zachos (2017), Orbital forcing of the Paleocene and Eocene carbon cycle, *Paleoceanography*, 32, doi:10.1002/2016PA003054

## Our additional references:

- Akaike, H.: A new look at the statistical model identification, *IEEE transactions on automatic control*, 19, 716-723, 1974
- Burnham, K. P. and Anderson, D. R.: *Model selection and multimodel inference: a practical information-theoretic approach*, Springer, New York, 2003.
- Schwarz, G.: Estimating the dimension of a model, *The annals of statistics*, 6, 461-464, 1978
- Thomas, D. J., Zachos, J. C., Bralower, T. J., Thomas, E., and Bohaty, S.: Warming the fuel for the fire: Evidence for the thermal dissociation of methane hydrate during the Paleocene-Eocene thermal maximum, *Geology*, 30, 1067-1070, 2002

# Sensitivity of the Eocene Climate to CO<sub>2</sub> and Orbital Variability

John S. Keery<sup>1</sup>, Philip B. Holden<sup>1</sup>, Neil R. Edwards<sup>1</sup>

<sup>1</sup>School of Environment, Earth & Ecosystem Sciences, The Open University, Milton Keynes, MK7 6AA, UK

Correspondence to: John S. Keery (john.keery@open.ac.uk)

**Abstract.** The early Eocene, from about 56 Ma, with high atmospheric CO<sub>2</sub> levels, offers an analogue for the response of the Earth's climate system to anthropogenic fossil fuel burning. In this study we present an ensemble of 50 Earth system model runs with an early Eocene palaeogeography and variation in the forcing values of atmospheric CO<sub>2</sub> and the Earth's orbital parameters. ~~Two dimensional model output fields are reduced to scalar values through simple summarising algorithms and by singular value decomposition.~~ Relationships between ~~these scalar results~~ simple summary metrics of model outputs and the forcing parameters are identified by linear modelling, providing estimates of the relative magnitudes of the effects of atmospheric CO<sub>2</sub> and each of the orbital parameters on important climatic features, including tropical-polar temperature difference, ocean-land temperature contrast, ~~and~~ Asian, African and S. American monsoon rains, and climate sensitivity. Our results indicate that although CO<sub>2</sub> exerts a dominant control on most of the climatic features examined in this study, the orbital parameters also strongly influence important components of the ocean-atmosphere system in a greenhouse Earth. In our ensemble, atmospheric CO<sub>2</sub> spans the range 280 - 3000 ppm, and this variation accounts for over 9590% of the effects on mean air temperature, southern winter high-latitude ocean-land temperature contrast and northern winter tropical-polar temperature difference. However, the variation of precession accounts for over 8075% of the influence of the forcing parameters on the Asian and African monsoon rainfall, and obliquity variation accounts for over 65% of the effects on winter ocean-land temperature contrast in high northern latitudes, and northern summer tropical-polar temperature difference. Our results indicate a bimodal climate sensitivity, with values of 4.36°C and 2.54°C, dependent on low or high states of atmospheric CO<sub>2</sub> concentration respectively, with a threshold at approximately 1000 ppm in this model, and due to a saturated vegetation-albedo feedback. Our method gives a quantitative ranking of the influence of each of the forcing parameters on key climatic model outputs, with additional spatial information from ~~our~~ singular value decomposition ~~approach~~ providing insights into likely physical mechanisms. The results demonstrate the importance of orbital variation as an agent of change in climates of the past, and we demonstrate that emulators derived from our modelling output can be used as rapid and efficient surrogates of the full complexity model, to provide estimates of climate conditions from any set of forcing parameters.

## 1 Introduction

In the early Eocene several episodes of global warming coincided with carbon isotope excursions (CIEs), pulses of isotopically light carbon injected into the atmosphere and oceans, and recorded in high-resolution marine and terrestrial

1 sediments (Kennett and Stott, 1991). In one large CIE, at the Palaeocene-Eocene transition at ~56 Ma, the Palaeocene-  
2 Eocene Thermal Maximum (PETM), evidence from both tropical (e.g. Zachos et al., 2003) and polar (e.g. Sluijs et al., 2006)  
3 regions indicates that temperatures increased by ~5°C in less than 10 kyr. Although the greenhouse gas (GHG) sources, and  
4 the duration of the onset phase of the PETM are uncertain, the relatively short time scale and global extent of the PETM  
5 strongly suggest that a large and sudden increase in GHGs in the atmosphere was the primary climatic forcing factor (Zachos  
6 et al., 2007). Since the PETM is the most recent period in Earth's history for which estimated atmospheric GHG  
7 concentrations are similar in magnitude to those of the present-day, and expected to arise from~~Since estimates of GHG~~  
8 ~~emissions during the PETM are similar in magnitude to present day emissions produced by~~ fossil fuel burning, the PETM  
9 may provide a valuable analogue for anthropogenic climate change (e.g. McInerney and Wing, 2011; Zeebe et al., 2016;  
10 Zeebe and Zachos, 2013).

11 The CIEs of the early Eocene show similar regularity in their timing to periodic changes in the Earth's orbit around the sun  
12 (Lourens et al., 2005), and the search for causal relationships between orbital cycles and Paleogene climate is an active area  
13 of research (e.g. Lauretano et al., 2015; Laurin et al., 2016; Lunt et al., 2011).

14 Although the climatic state in the early Eocene cannot be directly measured, much information on temperature and  
15 biogeochemical conditions can be inferred from measurements of proxy data: preserved natural records of climate  
16 variability, which can be linked to the property of interest through physical processes (Jones and Mann, 2004). But there are  
17 major uncertainties in proxy data from the Eocene due to incomplete preservation and alteration over time, with additional  
18 uncertainties as to the seasonality of contributory processes, and for ocean proxies, the depth at which the property of  
19 interest, e.g. temperature, influences the proxy (Dunkley Jones et al., 2013). Climate models therefore have an important  
20 role to play in exploring the mechanistic functioning of palaeoclimates (Huber, 2012).

21 Climate simulations with high temporal and spatial resolution can be obtained from General Circulation Models (GCMs),  
22 but the requirement of GCMs for powerful computers and long run-times ~~precludes their use in~~ makes them difficult to  
23 deploy for large ensembles of model simulations and restricts their ability to investigate the large uncertainties in forcings  
24 and model parameterisations. Such ensembles are more practical with more heavily parameterised and hence more  
25 computationally efficient Earth system Models of Intermediate Complexity (EMICs), (Weber, 2010), although we note that  
26 Araya-Melo et al. (2015) and Lord et al. (2017) have deployed the GCM HadCM3 in ensemble-based studies of orbital  
27 forcing effects on climates of the Pleistocene and late Pliocene respectively.-

28 In this study we deploy an EMIC, PLASIM-GENIE (Holden et al., 2016), in an ensemble of model runs to investigate the  
29 effects of varying GHG concentration and orbital parameters on the palaeoclimate of the Earth, with an Eocene configuration  
30 of the oceans and continents. We reduce the dimensionality of the model output by computing simple scalar metrics to  
31 denote key climatic features of each ensemble member, and we apply singular value decomposition (SVD) to identify the  
32 principal components (PCs) of temperature and precipitation fields in the full ensemble, for comparison with the variation in  
33 the forcing parameters.

1 By applying the linear modelling [and emulation](#) methods of Holden et al. (2015), we regress both the simple scalar metrics  
2 and the SVD reduced dimension model outputs onto the forcing parameters, and from the derived relationships, we infer  
3 main effects ~~indices~~ denoting the effect of each explanatory term [in the linear model](#), and total effects ~~indices~~ denoting the  
4 effect of each forcing parameter, on the variation in the scalar metrics and on the temperature and precipitation output fields.  
5 [We demonstrate that emulators derived in respect of tropical precipitation metrics can be used to estimate Eocene monsoonal](#)  
6 [responses to any combination of GHG and orbital forcing parameter values.](#)

## 7 **2 The Early Eocene and the PETM**

### 8 [2.1 Climate of the Early Eocene](#)

9 During the Eocene, the Earth remained in the ‘greenhouse’ state, which had persisted since the early Cretaceous, with polar  
10 air temperatures remaining above 0°C for most of the year (Wing and Greenwood, 1993), no permanent polar ice-caps,  
11 reduced equator-pole temperature gradients, and lower ocean-land temperature contrasts, inferred from fossil and isotope  
12 indicators of temperature and environmental conditions. Climate modellers have experienced difficulty in simulating  
13 Cretaceous and Palaeogene ‘equable climates’ (Sloan and Barron, 1990; Wing and Greenwood, 1993) with sufficient  
14 warming at high latitudes, without overheating the tropics, although Huber and Caballero (2011), hereafter HC11, ~~have~~  
15 demonstrated that with sufficiently high levels of [CO<sub>2</sub> \(as a proxy for all forms of radiative forcing\)](#), climate models can  
16 generate global air temperature distributions in broad agreement with the proxy temperature measurements.

17 The onset of the PETM, at approximately 55.9 Ma (Westerhold et al., 2009), is recognised as the boundary between the  
18 Palaeocene and Eocene epochs (Aubry et al., 2007), and is characterised by a large CIE, indicating large GHG emissions,  
19 accompanied by a sudden rise in global temperature (Kennett and Stott, 1991), extensive extinction and origination of  
20 nannoplankton (Gibbs et al., 2006), and widespread ocean anoxia (Dickson et al., 2012). There is some evidence [from](#)  
21 [analysis and modelling of the timing and duration of variations in  \$\delta^{13}\text{C}\$  and  \$\delta^{18}\text{O}\$  observed in nannoplankton fossils](#) that some  
22 of the GHG emissions were initially in the form of CH<sub>4</sub> (Dickens, 2011; Lunt et al., 2011; Thomas et al., 2002), which is  
23 [rapidly](#) oxidised in the atmosphere to CO<sub>2</sub>. The PETM is also marked by enhanced precipitation and continental weathering  
24 (Carmichael et al., 2016; Chen et al., 2016; Penman, 2016), rapid and sustained surface ocean acidification (Penman et al.,  
25 2014; Zachos et al., 2005), and shares many features of the global-scale oceanic anoxic events of the Cretaceous and  
26 Jurassic periods (Jenkyns, 2010). See McInerney and Wing (2011) for a review of PETM research.

27 The duration of the onset phase of the PETM is uncertain. Cui et al. (2011) have suggested that the peak rate of addition of  
28 CO<sub>2</sub> to the atmosphere was much lower than the present-day rate of anthropogenic GHG emissions, but this is disputed by  
29 Sluijs et al. (2012). Zeebe et al. (2016) have estimated that the initial release of carbon at the onset of the PETM lasted at  
30 least 4 Ka, at a rate which was little more than one tenth of the present rate of anthropogenic emissions, so the Earth may  
31 already be in a ‘no-analogue’ state, with anthropogenic climate change likely to exceed that of the PETM. However rapid the

1 onset, the greenhouse conditions of the early Eocene, and particularly the PETM, provide an opportunity to apply lessons  
2 from the past, with a view to improving predictions of the future (Lunt et al., 2013).

### 3 **2.21 Palaeogeography of the Early Eocene**

4 ~~Although~~ The arrangement of the continents and oceans in the Early Eocene was broadly similar to that of the present, with  
5 the Earth's land mass divided into the same major continents, and with most of the land mass in the northern hemisphere.  
6 India had not yet collided with the Eurasian continent, and the closure of the Tethys Ocean was not yet complete. - Such  
7 tectonic movements may have effected some changes to the climate system. In particular, the configuration of ocean  
8 gateways strongly influences modes of ocean circulation, and hence affects energy transport throughout the climate system  
9 (Lunt et al., 2016; Sijp et al., 2014).

#### 10 **2.21.1 Continental and Ocean Configurations during the Early Eocene**

11 Although the Bering Strait was closed throughout the Palaeogene (Marincovich et al., 1990), and the Western Interior  
12 Seaway linking the Arctic to the Pacific was closed by the end of the Cretaceous (Slattery et al., 2015), the Arctic Ocean was  
13 connected to the major oceans during the early Eocene through the Turgai Strait, also known as the Western Siberian  
14 Seaway (Akhmetiev et al., 2012; Radionova and Khokhlova, 2000). The Lomonosov Ridge, from which core samples have  
15 been obtained by the Arctic Coring Expedition (ACEX) of the Integrated Ocean Drilling Program Expedition (IODP) 302  
16 (Backman et al., 2008), was on the edge of the Arctic basin rather than across the pole as in the present configuration  
17 (O'Regan et al., 2008).

18 Both the Drake Passage between South America and Antarctica (Barker and Burrell, 1977) and the Tasman Gateway  
19 between Australia and Antarctica (Exon et al., 2004) were closed during the early Eocene, preventing the development of an  
20 Antarctic Circumpolar Current and allowing greater southern hemisphere meridional heat transport than in the modern  
21 world.

#### 22 **2.12.2 Orbital Configurations**

23 Throughout Earth's geological history, oscillations in the relative positions of the Earth and Sun have influenced both the  
24 Earth's climate, and rates of sedimentation in some climate-sensitive environmental settings (Hinnov and Hilgen, 2012). The  
25 main oscillations are the eccentricity of the Earth's orbit around the Sun, with ~~dominant~~ periods of ~100 ka and ~4050 ka,  
26 the obliquity or tilt of the Earth's axis of rotation, with a period of ~40 ka, and precession, the relative timing between  
27 perihelion and the seasons, with a period of ~20 ka (Berger et al., 1993). By correlating oscillations preserved in the  
28 geological record with computed time series of changes in insolation received by the Earth, an absolute astronomical time  
29 scale may be constructed for recent time-spans with a complete sedimentary record, but where the geological evidence is  
30 incomplete, or where uncertainties in the orbital model are too great further back in time, only a relative time scale may be  
31 derived (Hilgen et al., 2010). An absolute astronomical time scalesolution has been computed back to 50 Ma (Laskar et al.,

1 2011), and an absolute age of  $55.53 \pm 0.05$  Ma has been proposed for the onset of the PETM at the start of the Eocene epoch  
2 by Westerhold et al. (2012).

3 Lourens et al. (2005) noted the apparent astronomical pacing of global warming events in the late Palaeocene and early  
4 Eocene, with correlations to both the long and short periods of eccentricity. Sexton et al. (2011) suggested that although the  
5 smaller hyperthermal events of the early Eocene were driven by cycles of carbon sequestration and release in the ocean,  
6 paced by the eccentricity cycles, the PETM was likely to have been driven by carbon injection from a sedimentary source.  
7 Laurin et al. (2016) applied a method which allows the phase of the  $\sim 4050$  Ka eccentricity cycle to be identified from  
8 interference patterns and frequency modulation of the  $\sim 100$  Ka eccentricity cycle, and concluded that four hyperthermals in  
9 the early Eocene were initiated at  $\sim 4050$  Ka eccentricity maxima, but in a study of terrestrial sediments with apparent  
10 correlation to the  $\sim 100$  Ka eccentricity cycle, Smith et al. (2014) suggested that hyperthermals occurred during eccentricity  
11 minima, rather than maxima.

12 ~~Ruddiman (2006) noted a relationship between obliquity and the extent of northern ice sheets, and also some correlation~~  
13 ~~between precession and northern summer monsoons, but this was thought to be related to feedbacks in the growth and decay~~  
14 ~~of ice sheets, and so may not be pertinent to the climate of the Eocene.~~

## 15 3 Methods

### 16 3.13 The PLASIM-GENIE Model

17  
18 PLASIM-GENIE (Holden et al., 2016) is an intermediate complexity AOGCM. We apply the model at a spectral T21  
19 atmospheric resolution, which corresponds to a triangular truncation applied at wave number 21 and a horizontal resolution  
20 of  $5.625^\circ$ , with 10 layers, and a matching ocean grid with 32 depth levels. We apply the calibrated parameter set of Holden  
21 et al (2016). The component modules are as follows:

22 PLASIM (Fraedrich, 2012) is built around the 3D primitive equation atmosphere model PUMA (Fraedrich et al., 2005). The  
23 radiation scheme considers two wavelength bands in the short wave and uses the broad band emissivity method for long  
24 wave. Fractional cloud cover is diagnosed. Other parameterised processes include large-scale precipitation, cumulus and  
25 shallow convection, dry convection and boundary layer heat fluxes.

26 GOLDSTEIN is a 3D frictional-geostrophic ocean model (Edwards and Marsh, 2005; Marsh et al., 2011), dynamically  
27 similar to classical GCMs, except that it neglects momentum advection and acceleration. Barotropic flow around the four  
28 continental islands (Fig. 1) is derived from linear constraints that arise from integrating the depth-averaged momentum  
29 equations.

30 GOLDSTEINSEAICE (Edwards and Marsh, 2005) solves for the fraction of the ocean surface covered by ice within a grid  
31 cell and for the average sea-ice height. A diagnostic equation is solved for the ice surface temperature. Growth or decay of

1 sea ice depends on the net heat flux into the ice (Hibler III, 1979; Semtner Jr, 1976). Sea-ice dynamics are represented by  
2 diffusion and advection by surface currents.

3 ENTS (Williamson et al., 2006) models vegetative and soil carbon densities, assuming a single plant functional type.  
4 Photosynthesis depends upon temperature (with a double-peaked response representing boreal and tropical forest),  
5 atmospheric CO<sub>2</sub> concentration and soil moisture availability. Self-shading is parameterised. Land surface albedo, moisture  
6 bucket capacity and surface roughness are parameterised in terms of the simulated carbon pool densities.

7 [The computational efficiency of PLASIM-GENIE is achieved mainly through low spatial resolution \(~5°\) and, relative to](#)  
8 [high-complexity Earth system models, simplifying assumptions in physical processes. These include, for instance,](#)  
9 [simplified parameterisations of radiative transport and convection in the atmosphere, the neglect of momentum transport in](#)  
10 [the ocean, and the representation of all vegetation as a single plant functional type. Climate sensitivity, the response of the](#)  
11 [climate to a doubling of atmospheric CO<sub>2</sub> concentration, including feedbacks, is an emergent property of the model.](#)

## 12 [4 Methods](#)

### 13 [3.21 Model Configuration](#)

#### 14 [3.21.1 Model Grid](#)

15 [This study was designed before Lunt et al. \(2017\) presented their 'DeepMIP' guidelines for model simulations of the latest](#)  
16 [Paleocene and early Eocene. However, our palaeogeography is based on the high-resolution digital reconstruction of the](#)  
17 [early Eocene published by Herold et al. \(2014\), and which Lunt et al. \(2017\) recommended should be used as the standard](#)  
18 [for all palaeoclimate simulations within the DeepMIP framework. We have used the dataset of Herold et al. \(2014\) published](#)  
19 [a high-resolution dataset of Eocene palaeogeography, which we have used](#) as an initial configuration for the tectonic layout,  
20 topography and bathymetric boundary conditions in our study. We have reduced the resolution of the Eocene  
21 palaeogeography provided by Herold et al. (2014) to a configuration of 64 longitude x 32 latitude cells, with each cell  
22 representing 5.625° in each orientation. Cells at high latitudes therefore represent smaller land areas than cells at low  
23 latitudes. Our vertical resolution is 32 ocean depths and 10 atmospheric layers. We have incorporated the ocean gateway  
24 configurations discussed in section 2.1.1. The Turgai Strait is open in our configuration, and is the only connection between  
25 the Arctic Ocean and other oceans. The Drake Passage and Tasman Gateway are both closed.

26 The palaeogeography (Fig. 1) comprises four land masses: N America and Eurasia; Antarctica combined with S America and  
27 Australia; Africa; and India. Red rectangles in Fig. 1 indicate the boundaries of areas used to calculate simple metrics of  
28 centennially averaged seasonal precipitation, as empirical indicators of African, Asian and S. American monsoons.

#### 29 [3.21.2 Forcing and Other Input Parameters](#)

30 In order to investigate the sensitivity of the Eocene climate to variation in atmospheric CO<sub>2</sub> and orbital parameters, we have  
31 constructed an ensemble of 50 model configurations, each with a unique set of forcing parameters comprising atmospheric

1 CO<sub>2</sub>, eccentricity ( $e$ ), obliquity ( $\epsilon$ ) and precession ( $\omega$ ), the angle on the Earth's orbit around the Sun between the moving  
2 vernal equinox and the longitude of perihelion (Berger et al., 1993). When  $e$  is zero, the Earth's distance from the Sun is  
3 constant at all points on the orbit, so there is no precessional effect. The magnitude of precessional effects is controlled by  $e$ ,  
4 while phase is controlled by  $\omega$ , so precessional effects are commonly described by the precession index given by  $e\sin\omega$ . The  
5 only orbital parameter which alters the total annual solar radiation received by the Earth is  $e$ , although the range of variation  
6 is very small. We include  $e$  and  $\omega$  as separate and independent forcing parameters, rather than combined as the precession  
7 index, or in the form  $e\cos\omega$ . This approach does not make the assumption that the only effect of eccentricity on the Earth's  
8 climate is through its effect on the amplitude of the precession cycle, but allows experimental results to be examined for  
9 effects of  $e$  and  $\omega$  either separately or in combination. ~~with a~~ An additional dummy parameter is included to test for  
10 possible overfitting of relationships between forcing parameters and model output fields.

11 Although the maximum ~~value~~ mass of CO<sub>2</sub> injected into the atmosphere during CIEs, and in particular the PETM, remains  
12 uncertain, there is broad agreement that the atmospheric concentration of CO<sub>2</sub> # did not exceed 3000 ppm (e.g. Gehler et al.,  
13 2016), and that it did not fall below the pre-industrial level of 280 ppm at any time during the early Eocene. We allocate  
14 these values as the limits of a uniform range from which our ensemble of CO<sub>2</sub> values is selected.

15 Since the absolute astronomical time scale for the early Eocene has an uncertainty which is greater than the periods of the  
16 obliquity and precession cycles, and there remains disagreement as to which phases of the eccentricity cycles are related to  
17 CIEs, there are no combinations of the orbital forcing parameters which can be known a priori to be of greater importance in  
18 their effects on the Eocene climate in general, and on their contributions to the initiation, duration and termination of the  
19 CIEs in particular. ~~We~~ we therefore select values of orbital parameters independently, and from the full range of each  
20 parameter's variation during the early Eocene.

21 To ensure the best coverage of the five-dimensional state-space comprised of the four forcing parameters and the additional  
22 dummy parameter in a limited number of model runs, we apply the Latin hypercube method (McKay et al., 1979), a  
23 constrained Monte Carlo sampling scheme in which the range to be sampled for each variable is divided into non-  
24 overlapping intervals, and one value from each interval is randomly selected (Wyss and Jorgensen, 1998). This provides  
25 adequate coverage of the state space more efficiently than can be achieved by a simple Monte-Carlo sampling approach  
26 (Rougier, 2007). The present study has been designed to facilitate direct comparison between the results for specific  
27 ensemble members and their direct counterparts in a future study using the EMIC model GENIE-1 (Edwards and Marsh,  
28 2005), which will include additional forcing parameters not used by this PLASIM-GENIE study. We have applied an  
29 iterative method to generate a pair of corresponding hypercubes with five and eleven dimensions for the PLASIM-GENIE  
30 and GENIE-1 studies respectively, in which the minimum Euclidean distance between any two points is maximised, and  
31 linear correlation between any two parameters is minimised. Details of the steps taken to generate the hypercubes are  
32 provided in Appendix A. The absolute value of the  $r$  correlation coefficient does# not exceed 0.1 for any pair of input

1 [\(forcing and dummy\) parameters](#). Uniform ranges for each of the forcing parameters and the dummy parameter are shown in  
2 Table 1, and the values applied in all 50 PLASIM-GENIE ensemble members are shown in Table 2.

3 The intensity of radiation emitted by the Sun has increased steadily over time, and we apply the linear model of [Gough](#)  
4 [\(1981\)](#), and select a solar constant of  $1358.68 \text{ W m}^{-2}$  ~~Gough (1981)~~. [We note that Lunt et al. \(2017\) have recommended that](#)  
5 [a modern value of  \$1361.0 \text{ W m}^{-2}\$  should be applied to studies within the DeepMIP framework, in order to facilitate](#)  
6 [comparison between simulations with modern and pre-industrial levels of  \$\text{CO}\_2\$ , and to offset the absence of elevated levels of](#)  
7  [\$\text{CH}\_4\$](#) .

### 8 **[3.21.3](#) Running the Models**

9 Each simulation was run for [a spin-up period of](#) 1000 years to reach a quasi-steady state, with key output fields recorded as  
10 seasonal averages for each of the three-month periods December, January and February (DJF) and June, July and August  
11 (JJA), representing both winter and summer seasons in both the northern and southern hemispheres. Although model output  
12 includes time series of some fields and output values every 100 years, in this study only the field values recorded at the end  
13 of the 1000 years of modelling are used for analysis of the results.

### 14 **[3.32](#) Analysis of Model Output**

15 Comparison of the forcing parameters applied in the ensemble with the model output fields can be more efficiently achieved  
16 by reducing the dimensionality of the model output while retaining information on key components of the climate system.

#### 17 **[3.32.1](#) Simple Metrics**

18 In studies of the Earth's modern climate, it is recognised that the tropical-polar temperature difference (TPTD) influences  
19 poleward energy flux, and the ocean-land temperature contrast (OLC) affects monsoon intensity (Jain et al., 1999; Karoly  
20 and Braganza, 2001; Peixoto and Oort, 1992). Although atmospheric circulation patterns in the early Eocene ~~are likely to will~~  
21 have differed from those in the modern world, in selecting latitude regions to represent the TPTD, we adopt the approach of  
22 Abbot and Tziperman (2008), who configured their model of the Cretaceous climate with latitude ranges of  $0\text{--}30^\circ$ ,  $30\text{--}60^\circ$ ,  
23 and  $60\text{--}90^\circ$ , the approximate boundaries of the Hadley, Ferrel and Polar cells observed in the modern world (Peixoto and  
24 Oort, 1992). On our model grid in which each cell spans  $5.625^\circ$  of latitude, for the purposes of deriving scalar metrics, we  
25 define the tropical regions to be between  $0.0^\circ$  and  $33.75^\circ$  North and South, and the polar regions to be between  $56.25^\circ$  to  $90^\circ$   
26 North and South.

27 From the output values of air temperature in the lowest level of the atmosphere, weighted by grid cell area, we derive scalar  
28 values for each model run, of global annual mean air temperature (MAT), northern and southern hemisphere seasonality  
29 (mean area-weighted DJF-JJA temperature differences in the above-defined polar regions), TPTD for summer and winter in  
30 each hemisphere, and ~~ocean-land temperature contrast~~OLC for summer and winter in tropical and polar regions in each  
31 hemisphere.

1 Monsoons are related to seasonal variations in tropical and subtropical winds and precipitation (Trenberth et al., 2006).  
2 Wang and Fan (1999) noted that the choice of an index to denote monsoon behaviour in the modern world is difficult and  
3 arbitrary, with commonly applied indices based on average summer precipitation, maximum summer precipitation, winter-  
4 summer difference in precipitation, or wind circulation patterns within defined geographical areas. In this study, we derive  
5 simple scalar metrics to denote indices for monsoons for Asia, Africa and South America ~~from the difference in by~~  
6 ~~subtracting winter rainfall from summer~~ rainfall ~~in DJF and JJA~~, for defined geographical regions, denoted on Fig. 1, and  
7 selected for their similarity to monsoonal regions in the modern continental configuration.

### 8 **3.32.2 Singular Value Decomposition, Linear Modelling and Model Emulation**

9 We ~~perform a singular value decomposition to identify the~~~~apply the linear algebraic tool SVD to identify the~~ PCs and  
10 empirical orthogonal functions (EOFs) of temperature and precipitation fields in the full ensemble ~~, although we note that~~  
11 ~~climate variability may not be due to physical processes which vary orthogonally, and identification of PCs can be~~  
12 ~~influenced by aspects of the experimental design~~. A detailed presentation of the use of this method in the analysis of climate  
13 data is given by Hannachi (2004).

14 We use the linear modelling method of Holden et al. (2015), to regress both the simple scalar metrics and the SVD reduced  
15 dimension model outputs onto the forcing parameters. Values of the forcing parameters CO<sub>2</sub>, ~~e-eccentricity~~ and ~~obliquity-g~~  
16 (with its very small angular range considered to be approximately linear) were normalised to the ~~same~~ range [-1, 1] ~~as the~~  
17 ~~sines and cosines of precession values and combined with sin $\omega$  and cos $\omega$~~ , to form ~~a~~ 50-element column vectors ~~for~~  
18 ~~each representing the~~ forcing factors. Each 2-D (32 x 64) result field for each ensemble member was unrolled to form a  
19 column vector of 2048 elements, comprising a single column within a 2048 x 50 matrix of full ensemble values.

20 SVD was applied to decompose the full ensemble matrix for each 2-D result field, providing a 2048 x 50 matrix of PCs, a 50  
21 x 50 matrix of PC scores, and a 50 x 50 matrix of diagonal values.

22 Linear modelling was applied to determine relationships between the normalised forcing factors and the first six columns of  
23 the PC scores, including products of pairs of forcing factors, and squares of each forcing factor, with the best fitting  
24 relationships selected according to the Akaike information criterion (Akaike, 1974) then refined using Bayes information  
25 criterion (Schwarz, 1978). ~~Burnham and Anderson (2003) provide a detailed discussion of the application of information~~  
26 ~~criteria in model selection~~. The resulting relationship provides a simple emulator which can be used to estimate a PC score  
27 for the 2-D model field, given a single set of forcing parameter values. Applying derived emulators in respect of temperature  
28 and precipitation for both seasons, demonstrated high correlation between emulated PC scores and PC scores derived  
29 directly through SVD (Table 23).

30 ~~Our emulator approach uses linear regression, rather than a Gaussian process (GP), and is therefore simpler than the~~  
31 ~~methods~~~~A similar emulator approach has been~~ applied by ~~Bounceur et al. (2015)~~ Bounceur et al. (2015) in a study of the  
32 response of the climate-vegetation system in interglacial conditions to astronomical forcing, ~~and by~~ Araya-Melo et al. (2015)  
33 ~~in their study of the Indian monsoon in the Pleistocene~~. ~~Total effects indices, which denote the effect of each forcing~~

parameter on the full ensemble variation in the scalar metrics and on the temperature and precipitation output fields, are inferred from the derived relationships. Unlike linear models, GP models are intrinsically stochastic and give a more accurate quantification of their own error in emulating the input data. However, GP models can become computationally demanding in high dimensional space, and their results can be more difficult to interpret.

In order to analyse the results of each of our linear models, we apply the method described in detail by Holden et al. (2015) to derive the main effects (Oakley and O'Hagan, 2004), which provide a measure of the variation in the linear model output due to each of the terms (first order, second order and cross products), derived from their coefficients, and total effects (Homma and Saltelli, 1996), which separate the effect of each forcing parameter on the variation in the model output. Although the forcing factors are all scaled within the range [-1, 1], the trigonometrical precession terms are not uniformly distributed across this range. We have therefore computed the variances of the first order, second order and cross product terms directly for all parameters, rather than applying the respective approximations of  $\frac{1}{3}$ ,  $\frac{1}{9}$  and  $\frac{4}{45}$ , and we have applied these values as scaling factors in calculating the main effects and total effects.

## 5.4 Results

### 4.1 Model Output - Temperature and Precipitation

Analysis of the model results has focused on variation in surface air temperature and precipitation in both winter and summer in each hemisphere, although it should be noted that our experiment has not been designed such that mean values in our ensemble output represent direct estimates of the Eocene climate mean. In the left column of Fig. 2, median temperatures at each grid cell for the full ensemble are plotted for DJF (top) and for JJA (bottom), with the standard deviations plotted in the right column.

Ranges of median temperatures over land are greater than over the oceans, but TPTD is smaller in both seasons and both hemispheres than simulated in the modern world (see Fig. 2, Holden et al 2016). It is apparent from the standard deviation field that the tropical-polar temperature difference varies substantially across the ensemble, particularly in northern winter. The temperature distributions are similar to those of the 2240 ppm CO<sub>2</sub> simulation of HC11, regarded as their “mid to late Eocene” analogue (they consider elevated CO<sub>2</sub> as a proxy for all radiative forcing, including uncertain climate sensitivity). The principal difference is in high northern latitude winter temperatures; the Arctic ocean remains above freezing in HC11. We note that the Arctic winter median air temperature is below freezing over both land and sea in the PLASIM-GENIE ensemble, (see SST plots in Fig 3) and the Arctic does not remain ice-free throughout the year in any of the 50 simulations in our study. Tropical temperatures in excess of 35°C were simulated in some cases, as in HC11, which they regarded as their “most troubling result”, although they note observational data is currently insufficient to rule this out. Finally, we note that multi-model ensembles have found significant inter-model differences including, for instance a 9°C spread in global average temperature under the same CO<sub>2</sub> forcing (Lunt et al 2012). Quantification of model-related uncertainty is beyond the scope

1 ~~of the present study. A future analysis of PLASIM-GENIE parametric uncertainty is anticipated, but beyond the scope of this~~  
2 ~~paper.~~

3 Full ensemble distributions of mean latitudinal distributions of annual mean sea surface temperature (SST), with mean  
4 latitudinal distributions of maritime and continental surface air temperature in both DJF and JJA are plotted in Fig. 3,  
5 together with ensemble medians and 5% and 95% percentiles of global annual mean SST, and maritime surface air  
6 temperature in both DJF and JJA. The greater range of temperatures below rather than above median values reflects our use  
7 of a uniform range of CO<sub>2</sub> forcing values, and the logarithmic response of temperature to increasing CO<sub>2</sub> concentration.  
8 There is substantial variation of mean temperature across the ensemble, around 20 degrees over land, but the temperature  
9 offset varies little with latitude outside of polar regions where snow and ice greatly reduce winter temperatures in the colder  
10 simulations. The variation in TPTD across the ensemble thus appears to be essentially driven by the strength of snow and ice  
11 albedo feedbacks.

12 Our ensemble distributions of sea and air temperatures are in broad agreement with the values from the Eocene model  
13 studies compared by Lunt et al. (2012), [hereafter L12](#), and with the tables of marine and terrestrial proxy data compiled by  
14 ~~Lunt et al. (2012)~~[L12](#) and HC11, ~~but it should be noted that these proxy data spanned the entire Eocene era covering the early~~  
15 ~~Eocene, and including some records from the very latest Paleocene, but not including the PETM.~~ Our palaeogeography  
16 specifically represents the early Eocene, but our range of CO<sub>2</sub> and orbital inputs is more representative of the variation in  
17 forcing across the whole era. [L12 have summarised variations of SST with latitude from their proxy data set, in their Fig. 1,](#)  
18 [including large error bars representing uncertainty which they attribute to assumptions about seawater chemistry, possible](#)  
19 [non-analogous behaviour between modern and ancient systems, and uncertainty in calibrations of relationships between](#)  
20 [proxy data and properties of the palaeoclimate. Our median values of SST are close to the median estimates of SST in L12](#)  
21 [at mid latitudes, and well within the uncertainty indicated by error bars at high latitudes.](#)

22  
23 Median values and standard deviations of precipitation at each grid cell are plotted in Fig. 4. Higher precipitation values and  
24 variation are largely confined to the tropics, especially to regions associated with monsoons in the present day: Africa and S.  
25 America in DJF, and S.E. Asia in JJA.

## 26 [4.2 Simple Metrics](#)

27 In Figs. 5 and 6, CO<sub>2</sub>, obliquity ( $\epsilon$ ) and precession index ( $esin\omega$ ) are plotted against MAT, northern seasonality, northern  
28 winter TPTD and northern summer TPTD (Fig. 5), and southern winter polar OLC, northern winter polar OLC, Asian  
29 monsoon index, ~~and~~ African monsoon index [and American monsoon index](#) (Fig. 6). [Subplots for obliquity and precession](#)  
30 [index in Figures 5 and 6 denote the CO<sub>2</sub> level on a continuous colour scale.](#) The dominant effect of CO<sub>2</sub> on MAT and  
31 northern seasonality is apparent in Fig. 5, and it can also be seen that CO<sub>2</sub> strongly affects the northern TPTD in the winter,  
32 but not in the summer, when the combined influence of obliquity and precession index is discernible, suggesting that  
33 temperature proxies with seasonal bias may have a significant orbital imprint. The plot of atmospheric CO<sub>2</sub> against N.

1 Winter TPTD shows a change in gradient at approximately 1000 ppm CO<sub>2</sub> and 32°C. This may be related to the logarithmic  
2 dependence of radiative forcing on CO<sub>2</sub> concentration, ~~as well as~~ the disappearance of ice above some threshold level, ~~cf Fig.~~  
3 ~~3,~~ and a minimum level of land surface albedo related to maximum vegetation cover. A possible sea ice related threshold  
4 mechanism influencing both SST and maritime air temperature in high northern latitudes may be observed in Fig. 3, and this  
5 is strongly associated with the increase in northern winter TPTD at low CO<sub>2</sub> levels. Zeebe et al. (2017) have analysed a high  
6 resolution benthic isotope record covering the late Palaeocene - early Eocene, and have concluded that orbitally paced cycles  
7 are unlikely to have been driven by high latitude mechanisms, but our PLASIM-GENIE modelling suggests that while  
8 northern TPTD is not orbitally paced in the winter, being controlled by CO<sub>2</sub>, it is orbitally paced in the summer, by a  
9 combination of obliquity and precession.

10 It can be observed in Fig. 6 that there is strong correlation between CO<sub>2</sub> and southern winter polar OLC. The African and  
11 Asian monsoon indices are both correlated with the precession index, a well established feature of Quaternary records (e.g.  
12 Cruz et al., 2005). The American monsoon index is fairly strongly correlated with the precession index at high levels of  
13 CO<sub>2</sub>, and negatively correlated with CO<sub>2</sub> at low levels of CO<sub>2</sub>. In each of ~~these the other~~ examples, there is no apparent  
14 correlation between the simple metric and two of the three forcing factors. We have selected these simple metrics with  
15 visible correlations to the forcing parameters for further analysis with the linear modelling and emulation methods. Total  
16 effects on the simple metrics have been calculated for each of the forcing parameters, with eccentricity and precession  
17 considered separately, rather than combined within the precession index, and are shown in Table ~~43~~.

18 The total effects of CO<sub>2</sub> on MAT, northern winter TPTD and southern winter polar OLC, and of precession on both the  
19 Asian and African monsoon indices are all very high (> 0.90~~5~~), and the total effects of obliquity on northern winter polar  
20 OLC and northern summer TPTD, ~~and of precession on both the Asian and African monsoon indices~~ are ~~both~~ fairly high  
21 (> 0.65), providing quantitative confirmation of the correlations visible in Figs. 5 and 6.

### 22 4.3 Climate Sensitivity and Mean Air Temperature

23 Figure 7 shows the relationship between CO<sub>2</sub> (plotted on a logarithmic scale), and MAT, with an abrupt change of gradient  
24 clearly visible at a CO<sub>2</sub> concentration of 1000 ppm. From the two gradients, we derive climate sensitivity values for a  
25 doubling of CO<sub>2</sub> concentration at CO<sub>2</sub> levels below 1000 ppm, and at CO<sub>2</sub> levels above 1000 ppm, of 4.36°C and 2.54°C  
26 respectively. We note that our modelled values of carbon in vegetation in the ENTS module remain low outside of the  
27 tropics at low CO<sub>2</sub> concentration, but as CO<sub>2</sub> concentration increases, land areas at higher latitudes reach maximum values of  
28 carbon in vegetation, with all land areas showing no further capacity for increased carbon in vegetation at an atmospheric  
29 concentration of ~1000 ppm. The increase in land vegetation cover, with corresponding reduction in albedo, ~~appears to~~ acts  
30 as a positive feedback to rising temperature caused by increasing CO<sub>2</sub>, but this feedback mechanism ceases to operate when  
31 all available land is at its maximum vegetation capacity, with a consequent reduction in the climate sensitivity.

32 For a pre-industrial atmospheric CO<sub>2</sub> concentration of 280 ppm, the value of MAT indicated by our results for our early  
33 Eocene palaeogeography is 14.0°C. Holden et al. (2016) applied an identically configured PLASIM-GENIE to a modern

1 [geography, and their results show that with a pre-industrial CO<sub>2</sub> concentration, the model climate sensitivity is 3.8°C, and](#)  
2 [MAT is 12.9°C.](#)

3 [Our results also indicate values of global MAT for double, and four-times pre-industrial levels of CO<sub>2</sub> of 18.5°C and 22.5°C](#)  
4 [respectively; both these values are within the ranges of results for land near-surface air temperature in the modelling studies](#)  
5 [compared by L12, and shown in their Fig. 2b.](#)

#### 6 [4.4 Singular Value Decomposition](#)

7 Figure [7-8](#) shows the first three PCs of surface air temperature in DJF and JJA, with the percentages of temperature variation  
8 explained by each PC. Each of these plots illustrates the PC scaled by the standard deviation of the PC scores, thereby  
9 reflecting the variability across the ensemble. Note the variable scales for each of the subplots. In both DJF and JJA, PC1  
10 explains over 95% of the variance, with TPTD clearly visible in both hemispheres in DJF, but apparent only in the southern  
11 hemisphere in JJA. OLC is apparent in the plots of PC1 in both DJF and JJA. OLC is discernible in PC2 for DJF  
12 temperature, which explains 2.4% of variance, but less apparent, at least in the southern hemisphere, for JJA temperatures, in  
13 which PC2 explains 2.6% of the variance. For temperature in both DJF and JJA, PC3 explains less than 1% of the variance,  
14 with some indication of TPTD and OLC in DJF, but only of weak OLC at high latitudes in JJA. It is worth noting that even  
15 though lower order PCs explain small percentages of global variances, these PCs are generally associated with specific  
16 regions where they are comparably important to the first PC.

17 In their presentation of the SVD method applied in this study, Holden et al. (2015) investigated the effects of orbital  
18 parameters on the Earth's climate in the present day, but without including CO<sub>2</sub> as a forcing parameter in their ensemble, and  
19 found that obliquity had a dominant effect on the PC score of annual average surface air temperature. In our study of the  
20 Eocene climate, CO<sub>2</sub> is strongly correlated with N. seasonality (Fig. 5), and obliquity is weakly correlated with TPTD in ~~JJA~~  
21 [JJA](#) (Fig. 5) and with OLC in DJF (Fig. 6). The first three PCs of precipitation in DJF and JJA are shown in Fig. [89](#). PC1  
22 explains approximately 55% of the variance in both seasons, with PC2 and PC3 explaining over 20% and over 5%  
23 respectively, in both seasons. In both PC2 and PC3, areas of high seasonal contrast appear to correspond to areas which  
24 experience monsoons in the modern world.

25 Correlations between the PC scores of temperature and precipitation are provided in Table [54](#). The first PC scores of  
26 temperature, reflecting a global warming signal, are highly correlated with the first PC scores for precipitation, suggesting  
27 that these PCs reflect a strengthening of the hydrological cycle in response to warming. Similar considerations reveal  
28 connections between lower order PC scores, though we note that the 2<sup>nd</sup> (3<sup>rd</sup>) component of DJF temperature is associated  
29 with the 3<sup>rd</sup> (2<sup>nd</sup>) component of DJF precipitation. In order to address the drivers of these modes, we first consider the  
30 correlation coefficients,  $r$ , between forcing factors and the PC scores, shown in Table [65](#). These demonstrate that for each  
31 output there is a mode of variability driven by CO<sub>2</sub> and another mode driven by precession, suggesting they reflect global  
32 warming (and associated hydrological strength) and precessional forcing of the monsoon system.

1 There is strong correlation ( $r^2 > 0.5$ ) between CO<sub>2</sub> and the first PC scores of temperature in DJF and JJA. There are also  
2 strong correlations between precession index and the third PC scores for DJF temperature, and between precession index and  
3 the second PC scores for JJA temperature.

4 CO<sub>2</sub> is strongly correlated with the first PC scores of precipitation in both DJF and JJA, and there is a strong relationship  
5 between precession index and the second PC scores of precipitation in both DJF and JJA. An increase in the second PC  
6 scores for JJA precipitation in the Asian monsoon region (Fig. 9) corresponds to a decrease in the second PC scores for JJA  
7 temperature (Fig. 8), and as already noted, the second PC scores for both temperature and precipitation in JJA are strongly  
8 correlated to the precession index. This temperature reduction during the Asian monsoon was also observed by Holden et al.  
9 (2014), and attributed to a reduction in incoming solar radiation associated with increased cloud cover and surface  
10 evaporation.

#### 11 4.5 Linear Modelling and Emulation

12 The relationships between the forcing parameters (with precession expressed as both  $\sin \omega$  and  $\cos \omega$ ) and the simple metrics,  
13 and between the forcing parameters and the PC scores of 2-D fields, derived through linear modelling, include first and  
14 second order terms of forcing factors, together with products of forcing factors. In all cases most of the main effects are  
15 confined to the first order terms, and in no case does eccentricity have a significant effect independently of either of the  
16 precession terms, the effect of which eccentricity always augments slightly. All significant effects of the precession terms  
17 are accompanied by a small effect of eccentricity.

18 In Fig. 10, we ~~therefore neglect the higher order terms and~~ plot the ~~emulator coefficients of the first order terms (also termed~~  
19 ~~the 'main effects')~~ of the forcing parameters on the first three PCs of temperature and precipitation for DJF. Figure 11 shows  
20 the main effects of the forcing parameters on the first three PCs of temperature and precipitation plotted for JJA.

21 In both seasons, PC1 for temperature and precipitation can be almost entirely explained by CO<sub>2</sub>, reinforcing the earlier  
22 conclusion that these describe a connected mode, global warming with associated effects on the hydrological cycle. The  
23 main effects also suggest connections between the modes of variability of temperature and precipitation in lower-order  
24 components. In both seasons, and apparent in both variables, -there is a mode that is driven by precession; we interpret this  
25 as a monsoon signal, given precessional forcing and spatial patterns of rainfall that are characteristic of modern monsoons  
26 (Figs. 7-8 and 89). In JJA this is the second component of both variables. The mode is associated with precipitation  
27 variability of ~2.5 mm/day and temperature variability of ~3°C, with increased precipitation associated with a surface air  
28 cooling (note the negative correlation in Table 3, so that positive change in one field is associated with negative change in  
29 the other). In both cases, the local magnitude of variability is comparable to that driven by CO<sub>2</sub>. In DJF the precessional  
30 signal is again apparent in the second mode of precipitation, but the third mode of temperature. This mode is notable, in that  
31 it drives changes in simulated precipitation over East Africa (5 mm/day) that exceed CO<sub>2</sub>-driven variability. The remaining  
32 modes are more complex, and may not represent a clear mode of variability that can be straightforwardly attributed. For

1 instance, the third-order mode of JJA temperature is driven by an interaction between CO<sub>2</sub> and obliquity, but in precipitation  
2 can be explained ~~almost exclusively~~ by a combination of precession and CO<sub>2</sub>.

3 We apply the linear models derived from the forcing factors and monsoon indices as emulators to estimate values of  
4 monsoon indices corresponding to the full range of precession ( $\omega$ ), with eccentricity fixed at its high limit of 0.06, low and  
5 high values of CO<sub>2</sub> (300 ppm and 3000 ppm), and low and high values of obliquity (22.0° and 24.5°). Precession index  
6 ( $e\sin\omega$ ) and emulated values of the Asian, African and American monsoon indices are plotted in Figures 12, 13 and 14  
7 respectively. Relationships between the precession index and the monsoon indices which are visually suggested in Figure 6  
8 are shown with clear structure in Figures 12, 13 and 14. In each of the monsoon areas, the increase in precipitation due to  
9 precession effects is more pronounced at high atmospheric concentration of CO<sub>2</sub>, and also at high obliquity.

## 11 **6-5 Summary and Conclusions**

12 Our ensemble of 50 model runs of the EMIC PLASIM-GENIE has used an early Eocene palaeogeography incorporating  
13 recent understanding of the configuration of the continents and ocean gateways, with climate forcing by a randomly selected  
14 combination of atmospheric GHG emissions and orbital parameters for each model run. Relationships between forcing  
15 parameters and scalar summaries of model results have been derived through linear modelling.

16 Given the input range of CO<sub>2</sub>, our results show that, at the global scale, variability in patterns of surface air temperature is  
17 strongly dominated by a single mode of variation with a strong imprint of TPTD, focused in northern winter, that is entirely  
18 controlled by CO<sub>2</sub> (> 95% variance in both seasons). We note, however, that regions under the influence of monsoon  
19 systems exhibit precession-driven temperature variability that is comparable in magnitude to the variability driven by CO<sub>2</sub>  
20 (in large part the high proportion of variance explained by the CO<sub>2</sub> mode arises because the signal is global). In contrast to  
21 the unimodal dominance of CO<sub>2</sub> on the modelled global temperature fields, precipitation shows a somewhat more nuanced  
22 response. The first mode of precipitation, while still controlled entirely by CO<sub>2</sub>, is much less dominant (maximum 57%  
23 variance in DJF of 21% for PC2). In the second and third spatial modes of precipitation variability, CO<sub>2</sub> is still important, but  
24 no more so than orbital parameters, with PC2 controlled more strongly by precession index.

25 The importance of orbital forcing to precipitation signals is seen more clearly in the OLC and monsoon indices. In spite of  
26 large variation in atmospheric CO<sub>2</sub>, variation in obliquity accounts for well over half of the variation in high northern latitude  
27 ocean-land temperature contrast, and the variation in precession ~~strongly influences~~ is the dominant influence on seasonal  
28 variation in precipitation in tropical Africa and Asia, and combines with CO<sub>2</sub> to influence seasonal precipitation in tropical  
29 America. Our results strongly suggest the presence of monsoons in the early Eocene, but these climatic features would have  
30 developed without the effects of orography and high altitude plateau heating which are important factors in the modern south  
31 Asian monsoon (Boos and Kuang, 2010).

1 We note that the relative amplitude of the CO<sub>2</sub>-driven modes depends critically on the actual amplitude of CO<sub>2</sub> variability in  
2 the period of interest. While the ranges for orbital parameters are well defined, this is less true of CO<sub>2</sub> variability over the  
3 Eocene. If atmospheric CO<sub>2</sub> remained within a narrower range throughout the period, for example in the range 700 to 1800  
4 ppm, indicated for the early Eocene by Anagnostou et al. (2016) in a recent study using boron isotopes, then ~~and~~ outside of  
5 short-lived hyperthermals, the relative influence of CO<sub>2</sub> and orbital inputs might have been more evenly balanced. ~~We have~~  
6 ~~carried out an additional SVD of the 23 ensemble members with CO<sub>2</sub> in the range 700 to 1800 ppm, indicated for the early~~  
7 ~~Eocene by Anagnostou et al. (2016) in a recent study using boron isotopes. This analysis allocates 91% (86%) of the DJF~~  
8 ~~(JJA) SAT variance and 55% (48%) of the DJF (JJA) precipitation variance to the first (CO<sub>2</sub>-driven) principal components~~  
9 ~~thus, for global temperature patterns, the orbitally driven components contribute around twice as much variance as in the full~~  
10 ~~ensemble.~~

11 Our modelling results suggest that climate sensitivity is state dependent, with a value of 4.36°C in a low CO<sub>2</sub> state, and  
12 2.54°C in a high CO<sub>2</sub> state, due to a positive feedback mechanism in which albedo reduces as vegetation increases to its  
13 maximum value when CO<sub>2</sub> concentration reaches 1000 ppm.

14 We have demonstrated that emulators derived from linear modelling of the PLASIM-GENIE ensemble results can be used as  
15 a rapid and efficient method of estimating climate conditions from any set of forcing parameters, without the need for further  
16 deployment of the EMIC.

17 PLASIM-GENIE is to our knowledge the most sophisticated climate model that has been applied to an ensemble of Eocene  
18 simulations, but we note that increasing computing power is now enabling ensembles of simulations with moderately higher  
19 resolution models, such as HadCM3 (3.75° × 2.5°) (e.g. Araya-Melo et al., 2015; Lord et al., 2017), to be run, although with  
20 some limitation in the model years in each simulation. It will never be possible to apply state of the art climate models to  
21 large ensembles because, given the continual striving for the highest possible resolution, single simulations with such models  
22 will always be at the limits of what is practicable with available computing power. EMICs therefore have an important role  
23 in furthering our understanding of past, present and future climate systems, and in the rapid identification of influencing  
24 factors and modes of response which may be targeted for study by slower but more powerful models.

25 Our study of the early Eocene climate and the PETM using PLASIM-GENIE has shown that variability in orbital parameters  
26 can exert significant climatic influence, particularly in regard to tropical temperature and precipitation, and they should not  
27 be ignored in modelling studies of climates of the past.

## 28 **Data Availability**

29 Details on access to the model code, and instructions on compiling the model are given in Holden et al. (2016).

## Appendix A Hypercube Generation

This study has been designed together with a future study using the EMIC model GENIE-1 (Edwards and Marsh, 2005). The GENIE-1 model will use all four of the forcing parameters and the dummy parameter, used in the present study, together with an additional six forcing parameters not used by the PLASIM-GENIE study. For PLASIM-GENIE we have run 50 simulations with five parameters, while in GENIE-1 we will run 100 simulations with 11 parameters, so that the number of runs in each ensemble is approximately 10 times the input dimension (Loeppky et al., 2012).

The overall design for both studies is based on a maximin Latin hypercube with 100 rows and 11 columns produced by repeatedly invoking the lhsdesign function in MATLAB (MathWorks), with the command:

```
hyperCube = lhsdesign(100, 11, 'criterion', 'maximin', 'iterations', 100);
```

to select from 100 iteratively generated hypercubes, the one which best fits the maximin criterion, i.e. where the minimum Euclidian distance between points in hyperspace is at a maximum. This MATLAB command is repeated until the absolute value of correlation between columns falls below a selected value, or until a selected number of attempts has been made. The ability of this ‘brute force’ approach to produce a hypercube which satisfies the maximin criterion, with the required low correlation between columns decreases rapidly with an increasing number of columns, and a decreasing target correlation, but in several minutes it can generate a hypercube with 100 rows, each representing a design point for an ensemble member, and 11 columns, each representing a forcing or dummy parameter, with correlation between any two parameters not exceeding 0.1.

We then modify the overall design by first picking a subset of 50 of the 100 design points to give good coverage of the PLASIM-GENIE subspace. We randomly select an initial point, and iteratively select from the remainder, without replacement, the point which provides the largest increase in the number of populated sectors across all the two-dimensional projections of PLASIM-GENIE parameter space defined by dividing each two-dimensional subspace into 6 x 6 equal sectors.

This defines a template comprising a 50-member subset of 11 parameter values.

Copying the template and discarding the six parameters which are only used in the GENIE-1 ensemble yields the final hypercube design for the PLASIM-GENIE ensemble, comprising 50 sets of five parameters.

A second copy of the template forms the top half of the GENIE-1 hypercube, and the bottom half is partially constructed by duplicating only the five PLASIM-GENIE parameters from the first 50 rows, with the remaining six parameters determined by choosing a previously unselected point, without replacement, from the initial 100 x 11 hypercube that maximises the Euclidean distance between the pair of points in the subspace of the remaining six parameters.

Following this procedure, the two hypercubes for the PLASIM-GENIE and GENIE-1 studies both show very good state-space coverage and low correlation, and each member of the PLASIM-GENIE ensemble has two corresponding members in

1 [the GENIE-1 ensemble, with identical values for the parameters in common, but widely differing sets of values for the](#)  
2 [parameters only used by GENIE-1.](#)

### 3 **Author Contribution**

4 J. Keery and P. Holden designed and prepared the ensemble configurations and analysed the model outputs with advice from  
5 N. Edwards. J. Keery prepared the manuscript with contributions from both co-authors.

### 6 **Competing Interests**

7 The authors declare that they have no conflict of interest.

### 8 **Acknowledgements**

9 The authors gratefully acknowledge support from NERC, with funding for project NE/K006223/1. [We are very grateful to](#)  
10 [the reviewers M. Crucifix and D. De Vleeschouwer, and to the editor A. Winguth, for their thorough and constructive](#)  
11 [comments which have helped to improve the manuscript.](#)

### 12 **References**

- 13 Abbot, D. S. and Tziperman, E.: A high-latitude convective cloud feedback and equable climates, *Q. J. Roy. Meteor. Soc.*,  
14 134, 165-185, doi.10.1002/qj.211, 2008
- 15 Akaike, H.: A new look at the statistical model identification, *IEEE transactions on automatic control*, 19, 716-723, 1974
- 16 Akhmetiev, M. A., Zaporozhets, N. I., Benyamovskiy, V. N., Aleksandrova, G. N., Iakovleva, A. I., and Oreshkina, T. V.:  
17 The Paleogene history of the Western Siberian seaway - A connection of the Peri-Tethys to the Arctic Ocean, *Austrian J.*  
18 *Earth Sci.*, 105, 50-67, 2012
- 19 Anagnostou, E., John, E. H., Edgar, K. M., Foster, G. L., Ridgwell, A., Inglis, G. N., Pancost, R. D., Lunt, D. J., and  
20 Pearson, P. N.: Changing atmospheric CO<sub>2</sub> concentration was the primary driver of early Cenozoic climate, *Nature*, 533,  
21 380-384, doi.10.1038/nature17423, 2016
- 22 Araya-Melo, P. A., Crucifix, M., and Bounceur, N.: Global sensitivity analysis of the Indian monsoon during the  
23 Pleistocene, *Clim. Past*, 11, 45, doi.10.5194/cp-11-45-2015, 2015
- 24 Aubry, M.-P., Ouda, K., Dupuis, C., Berggren, W. A., and Couvering, J. A. V.: The Global Standard Stratotype-section and  
25 Point (GSSP) for the base of the Eocene Series in the Dababiya section (Egypt), *Episodes*, 30, 271, 2007

1 Backman, J., Jakobsson, M., Frank, M., Sangiorgi, F., Brinkhuis, H., Stickley, C., O'Regan, M., Løvlie, R., Pälike, H.,  
2 Spofforth, D., Gattacecca, J., Moran, K., King, J., and Heil, C.: Age model and core-seismic integration for the Cenozoic  
3 Arctic Coring Expedition sediments from the Lomonosov Ridge, *Paleoceanography*, 23, doi.10.1029/2007PA001476, 2008  
4 Barker, P. and Burrell, J.: The opening of Drake passage, *Mar. Geol.*, 25, 15-34, 1977  
5 Berger, A., Loutre, M. F., and Tricot, C.: Insolation and Earth's orbital periods, *J. Geophys. Res.-Atmos.*, 98, 10341-10362,  
6 1993  
7 Boos, W. R. and Kuang, Z.: Dominant control of the South Asian monsoon by orographic insulation versus plateau heating,  
8 *Nature*, 463, 218-222, doi.10.1038/nature08707, 2010  
9 Bounceur, N., Crucifix, M., and Wilkinson, R.: Global sensitivity analysis of the climate–vegetation system to astronomical  
10 forcing: an emulator-based approach, *Earth System Dynamics*, 6, 205-224, doi.10.5194/esd-6-205-2015, 2015  
11 Burnham, K. P. and Anderson, D. R.: *Model selection and multimodel inference: a practical information-theoretic approach*,  
12 Springer, New York, 2003.  
13 Carmichael, M. J., Lunt, D. J., Huber, M., Heinemann, M., Kiehl, J., LeGrande, A., Loftson, C. A., Roberts, C. D., Sagoo,  
14 N., Shields, C., Valdes, P. J., Winguth, A., Winguth, C., and Pancost, R. D.: A model–model and data–model comparison for  
15 the early Eocene hydrological cycle, *Clim. Past*, 12, 455-481, doi.10.5194/cp-12-455-2016, 2016  
16 Chen, Z., Ding, Z., Yang, S., Zhang, C., and Wang, X.: Increased precipitation and weathering across the Paleocene-Eocene  
17 thermal maximum in central China, *Geochem. Geophys. Geosy.*, 17, 2286–2297, doi.10.1002/2016GC006333, 2016  
18 Cruz, F. W., Burns, S. J., Karmann, I., Sharp, W. D., Vuille, M., Cardoso, A. O., Ferrari, J. A., Silva Dias, P. L., and Viana,  
19 O.: Insolation-driven changes in atmospheric circulation over the past 116,000 years in subtropical Brazil, *Nature*, 434, 63-  
20 66, doi.10.1038/nature03365, 2005  
21 Cui, Y., Kump, L. R., Ridgwell, A. J., Charles, A. J., Junium, C. K., Diefendorf, A. F., Freeman, K. H., Urban, N. M., and  
22 Harding, I. C.: Slow release of fossil carbon during the Palaeocene-Eocene Thermal Maximum, *Nat. Geosci.*, 4, 481-485,  
23 doi.10.1038/NGEO1179, 2011  
24 Dickens, G. R.: Down the rabbit hole: Toward appropriate discussion of methane release from gas hydrate systems during  
25 the Paleocene-Eocene thermal maximum and other past hyperthermal events, *Clim. Past*, 7, 831-846, doi.10.5194/cp-7-831-  
26 2011, 2011  
27 Dickson, A. J., Cohen, A. S., and Coe, A. L.: Seawater oxygenation during the Paleocene-Eocene thermal maximum,  
28 *Geology*, 40, 639-642, doi.10.1130/G32977.1, 2012  
29 Dunkley Jones, T., Lunt, D. J., Schmidt, D. N., Ridgwell, A., Sluijs, A., Valdes, P. J., and Maslin, M.: Climate model and  
30 proxy data constraints on ocean warming across the Paleocene–Eocene Thermal Maximum, *Earth-Sci. Rev.*, 125, 123-145,  
31 doi.10.1016/j.earscirev.2013.07.004, 2013  
32 Edwards, N. R. and Marsh, R.: Uncertainties due to transport-parameter sensitivity in an efficient 3-D ocean-climate model,  
33 *Clim. Dynam.*, 24, 415-433, doi.10.1007/s00382-004-0508-8, 2005

1 Exon, N. F., Kennett, J. P., and Malone, M. J.: Leg 189 synthesis: Cretaceous–Holocene history of the Tasmanian Gateway.  
2 In: Proceedings of the Ocean Drilling Program, Scientific Results, 189, Exon, N. F., Kennett, J. P., and Malone, M. J. (Eds.),  
3 Ocean Drilling Program, College Station, TX 2004.

4 Fraedrich, K.: A suite of user-friendly global climate models: hysteresis experiments, *Eur. Phys. J. Plus*, 127, 1-9,  
5 doi.10.1140/epjp/i2012-12053-7, 2012

6 Fraedrich, K., Kirk, E., Luksch, U., and Lunkeit, F.: The portable university model of the atmosphere (PUMA): Storm track  
7 dynamics and low-frequency variability, *Meteorol. Z.*, 14, 735-745, doi.10.1127/0941-2948/2005/0074, 2005

8 Gehler, A., Gingerich, P. D., and Pack, A.: Temperature and atmospheric CO<sub>2</sub> concentration estimates through the PETM  
9 using triple oxygen isotope analysis of mammalian bioapatite, *P. Natl. Acad. Sci. USA*, doi: 10.1073/pnas.1518116113,  
10 2016. 201518116, doi.10.1073/pnas.1518116113, 2016

11 Gibbs, S. J., Bown, P. R., Sessa, J. A., Bralower, T. J., and Wilson, P. A.: Nannoplankton extinction and origination across  
12 the Paleocene-Eocene thermal maximum, *Science*, 314, 1770-1773, 2006

13 Hannachi, A.: A primer for EOF analysis of climate data. University of Reading, Reading, 2004.

14 Herold, N., Buzan, J., Seton, M., Goldner, A., Green, J., Müller, R., Markwick, P., and Huber, M.: A suite of early Eocene (~  
15 55 Ma) climate model boundary conditions, *Geosci. Model Dev.*, 7, 2077-2090, doi.10.5194/gmd-7-2077-2014, 2014

16 Hibler III, W.: A dynamic thermodynamic sea ice model, *J. Phys. Oceanogr.*, 9, 815-846, 1979

17 Hilgen, F. J., Kuiper, K. F., and Lourens, L. J.: Evaluation of the astronomical time scale for the Paleocene and earliest  
18 Eocene, *Earth Planet. Sc. Lett.*, 300, 139-151, doi.10.1016/j.epsl.2010.09.044, 2010

19 Hinnov, L. A. and Hilgen, F. J.: Chapter 4 - Cyclostratigraphy and Astrochronology. In: *The Geologic Time Scale 2012*,  
20 Gradstein, F. M., Ogg, J. G., Schmitz, M. D., and Ogg, G. M. (Eds.), Elsevier, Boston, 2012.

21 Holden, P., Edwards, N., Garthwaite, P., Fraedrich, K., Lunkeit, F., Kirk, E., Labriet, M., Kanudia, A., and Babonneau, F.:  
22 PLASIM-ENTSem v1. 0: a spatio-temporal emulator of future climate change for impacts assessment, *Geosci. Model Dev.*,  
23 7, 433-451, doi.10.5194/gmd-7-433-2014, 2014

24 Holden, P. B., Edwards, N. R., Fraedrich, K., Kirk, E., Lunkeit, F., and Zhu, X.: PLASIM–GENIE v1.0: a new intermediate  
25 complexity AOGCM, *Geosci. Model Dev.*, 9, 3347-3361, doi.10.5194/gmd-9-3347-2016, 2016

26 Holden, P. B., Edwards, N. R., Garthwaite, P. H., and Wilkinson, R. D.: Emulation and interpretation of high-dimensional  
27 climate model outputs, *J. Appl. Stat.*, 42, 2038-2055, doi.10.1080/02664763.2015.1016412, 2015

28 Homma, T. and Saltelli, A.: Importance measures in global sensitivity analysis of nonlinear models, *Reliability Engineering  
29 and System Safety*, 52, 1-17, 1996

30 Huber, M.: Progress in greenhouse climate modeling. In: *Reconstructing Earth’s Deep-Time Climate - The State of the Art  
31 in 2012*, Ivany, L. C. and Huber, B. T. (Eds.), The Paleontological Society, Boulder, CO, 2012.

32 Huber, M. and Caballero, R.: The early Eocene equable climate problem revisited, *Clim. Past*, 7, 603-633, doi.10.5194/cp-7-  
33 603-2011, 2011

1 Jain, S., Lall, U., and Mann, M. E.: Seasonality and interannual variations of Northern Hemisphere temperature: Equator-to-  
2 pole gradient and ocean-land contrast, *J. Climate*, 12, 1086-1100, 1999

3 Jenkyns, H. C.: Geochemistry of oceanic anoxic events, *Geochem. Geophys. Geosy.*, 11, doi.10.1029/2009GC002788, 2010

4 Jones, P. D. and Mann, M. E.: Climate over past millennia, *Rev. Geophys.*, 42, 2004

5 Karoly, D. J. and Braganza, K.: Identifying global climate change using simple indices, *Geophys. Res. Lett.*, 28, 2205-2208,  
6 2001

7 Kennett, J. and Stott, L.: Abrupt deep-sea warming, palaeoceanographic changes and benthic extinctions at the end of the  
8 Palaeocene, *Nature*, 353, 225-229, doi.10.1038/353225a0, 1991

9 Laskar, J., Fienga, A., Gastineau, M., and Manche, H.: La2010: a new orbital solution for the long-term motion of the Earth,  
10 *Astron. Astrophys.*, 532, A89, doi.10.1051/0004-6361/201116836, 2011

11 Lauretano, V., Littler, K., Polling, M., Zachos, J. C., and Lourens, L. J.: Frequency, magnitude and character of  
12 hyperthermal events at the onset of the Early Eocene Climatic Optimum, *Clim. Past*, 11, 1313-1324, doi.10.5194/cp-11-  
13 1313-2015, 2015

14 Laurin, J., Meyers, S. R., Galeotti, S., and Lanci, L.: Frequency modulation reveals the phasing of orbital eccentricity during  
15 Cretaceous Oceanic Anoxic Event II and the Eocene hyperthermals, *Earth Planet. Sc. Lett.*, 442, 143-156,  
16 doi.10.1016/j.epsl.2016.02.047, 2016

17 Loepky, J. L., Sacks, J., and Welch, W. J.: Choosing the sample size of a computer experiment: A practical guide,  
18 *Technometrics*, 2012. 2012

19 Lord, N. S., Crucifix, M., Lunt, D. J., Thorne, M. C., Bounceur, N., Dowsett, H., O'Brien, C. L., and Ridgwell, A.:  
20 Emulation of long-term changes in global climate: Application to the late Pliocene and future, *Climate of the Past*  
21 *Discussions*, 2017, 1-47, doi.10.5194/cp-2017-57, 2017

22 Lourens, L. J., Sluijs, A., Kroon, D., Zachos, J. C., Thomas, E., Röhl, U., Bowles, J., and Raffi, I.: Astronomical pacing of  
23 late Palaeocene to early Eocene global warming events, *Nature*, 435, 1083-1087, doi.10.1038/nature03814, 2005

24 Lunt, D., Elderfield, H., Pancost, R., Ridgwell, A., Foster, G., Haywood, A., Kiehl, J., Sago, N., Shields, C., and Stone, E.:  
25 Warm climates of the past—a lesson for the future?, *Philos. T. R. Soc.-A*, 371, 20130146, doi.10.1098/rsta.2013.0146, 2013

26 Lunt, D. J., Dunkley Jones, T., Heinemann, M., Huber, M., LeGrande, A., Winguth, A., Loftson, C., Marotzke, J., Roberts,  
27 C., and Tindall, J.: A model–data comparison for a multi-model ensemble of early Eocene atmosphere–ocean simulations:  
28 EoMIP, *Clim. Past*, 8, 1717-1736, doi.10.5194/cp-8-1717-2012, 2012

29 Lunt, D. J., Farnsworth, A., Loftson, C., Foster, G. L., Markwick, P., O'Brien, C. L., Pancost, R. D., Robinson, S. A., and  
30 Wrobel, N.: Palaeogeographic controls on climate and proxy interpretation, *Clim. Past*, 12, 1181-1198, doi.10.5194/cp-12-  
31 1181-2016, 2016

32 Lunt, D. J., Huber, M., Anagnostou, E., Baatsen, M. L. J., Caballero, R., DeConto, R., Dijkstra, H. A., Donnadieu, Y.,  
33 Evans, D., Feng, R., Foster, G. L., Gasson, E., von der Heydt, A. S., Hollis, C. J., Inglis, G. N., Jones, S. M., Kiehl, J.,  
34 Kirtland Turner, S., Korty, R. L., Kozdon, R., Krishnan, S., Ladant, J. B., Langebroek, P., Lear, C. H., LeGrande, A. N.,

1 Littler, K., Markwick, P., Otto-Bliesner, B., Pearson, P., Poulsen, C. J., Salzmann, U., Shields, C., Snell, K., Stürz, M.,  
2 Super, J., Tabor, C., Tierney, J. E., Tourte, G. J. L., Tripathi, A., Upchurch, G. R., Wade, B. S., Wing, S. L., Winguth, A. M.  
3 E., Wright, N. M., Zachos, J. C., and Zeebe, R. E.: The DeepMIP contribution to PMIP4: experimental design for model  
4 simulations of the EECO, PETM, and pre-PETM (version 1.0), *Geosci. Model Dev.*, 10, 889-901, doi.10.5194/gmd-10-889-  
5 2017, 2017

6 Lunt, D. J., Ridgwell, A., Sluijs, A., Zachos, J., Hunter, S., and Haywood, A.: A model for orbital pacing of methane hydrate  
7 destabilization during the Palaeogene, *Nat. Geosci.*, 4, 775-778, doi.10.1038/ngeo1266, 2011

8 Marinovich, L., Brouwers, E. M., Hopkins, D. M., and McKenna, M. C.: Late Mesozoic and Cenozoic paleogeographic and  
9 paleoclimatic history of the Arctic Ocean Basin, based on shallow-water faunas and terrestrial vertebrates. In: *The Geology*  
10 *of North America, L: The Arctic Ocean Region*, Grantz, A., Sweeney, J. F., and Johnson, G. L. (Eds.), Geological Society of  
11 America, 1990.

12 Marsh, R., Müller, S., Yool, A., and Edwards, N.: Incorporation of the C-GOLDSTEIN efficient climate model into the  
13 GENIE framework: "eb\_go\_gs" configurations of GENIE, *Geosci. Model Dev.*, 4, 957-992, doi.10.5194/gmd-4-957-2011,  
14 2011

15 MathWorks: <https://uk.mathworks.com/help/stats/lhsdesign.html>, last access: 17 August 2017.

16 McInerney, F. A. and Wing, S. L.: The Paleocene-Eocene Thermal Maximum: A perturbation of carbon cycle, climate, and  
17 biosphere with implications for the future, *Annu. Rev. Earth Pl. Sc.*, 39, 489-516, doi.10.1146/annurev-earth-040610-  
18 133431, 2011

19 McKay, M. D., Beckman, R. J., and Conover, W. J.: A comparison of three methods for selecting values of input variables in  
20 the analysis of output from a computer code, *Technometrics*, 21, 239-245, 1979

21 O'Regan, M., Moran, K., Backman, J., Jakobsson, M., Sangiorgi, F., Brinkhuis, H., Pockalny, R., Skelton, A., Stickley, C.,  
22 and Koç, N.: Mid-Cenozoic tectonic and paleoenvironmental setting of the central Arctic Ocean, *Paleoceanography*, 23,  
23 doi.10.1029/2007PA001559, 2008

24 Oakley, J. E. and O'Hagan, A.: Probabilistic sensitivity analysis of complex models: a Bayesian approach, *Journal of the*  
25 *Royal Statistical Society: Series B (Statistical Methodology)*, 66, 751-769, 2004

26 Peixoto, J. P. and Oort, A. H.: *Physics of Climate*, American Institute of Physics, New York, 1992.

27 Penman, D. E.: Silicate weathering and North Atlantic silica burial during the Paleocene-Eocene Thermal Maximum,  
28 *Geology*, doi: 10.1130/G37704.1, 2016. G37704. 37701, doi.10.1130/G37704.1, 2016

29 Penman, D. E., Hönisch, B., Zeebe, R. E., Thomas, E., and Zachos, J. C.: Rapid and sustained surface ocean acidification  
30 during the Paleocene-Eocene Thermal Maximum, *Paleoceanography*, 29, 357-369, doi.10.1002/2014PA002621, 2014

31 Radionova, E. and Khokhlova, I.: Was the North Atlantic connected with the Tethys via the Arctic in the early Eocene?  
32 Evidence from siliceous plankton, *GFF*, 122, 133-134, doi.10.1080/11035890001221133, 2000

33 Rougier, J.: Probabilistic inference for future climate using an ensemble of climate model evaluations, *Climatic Change*, 81,  
34 247-264, doi.10.1007/s10584-006-9156-9, 2007

1 Schwarz, G.: Estimating the dimension of a model, *The annals of statistics*, 6, 461-464, 1978

2 Semtner Jr, A. J.: A model for the thermodynamic growth of sea ice in numerical investigations of climate, *J. Phys.*  
3 *Oceanogr.*, 6, 379-389, 1976

4 Sexton, P. F., Norris, R. D., Wilson, P. A., Pälike, H., Westerhold, T., Röhl, U., Bolton, C. T., and Gibbs, S.: Eocene global  
5 warming events driven by ventilation of oceanic dissolved organic carbon, *Nature*, 471, 349-352, doi.10.1038/nature09826,  
6 2011

7 Sijp, W. P., Anna, S., Dijkstra, H. A., Flögel, S., Douglas, P. M., and Bijl, P. K.: The role of ocean gateways on cooling  
8 climate on long time scales, *Global Planet. Change*, 119, 1-22, doi.10.1016/j.gloplacha.2014.04.004, 2014

9 Slattery, J. S., Cobban, W. A., McKinney, K. C., Harries, P. J., and Sandness, A. L.: Early Cretaceous to Paleocene  
10 paleogeography of the Western Interior Seaway: The interaction of eustasy and tectonism. In: *Cretaceous Conference:  
11 Evolution and Revolution*, Bingle-Davis, M. (Ed.), Wyoming Geological Association, Casper, WY, 2015.

12 Sloan, L. C. and Barron, E. J.: "Equable" climates during Earth history?, *Geology*, 18, 489-492, 1990

13 Sluijs, A., Schouten, S., Pagani, M., Woltering, M., Brinkhuis, H., Damsté, J. S. S., Dickens, G. R., Huber, M., Reichert, G.-  
14 J., and Stein, R.: Subtropical Arctic Ocean temperatures during the Palaeocene/Eocene thermal maximum, *Nature*, 441, 610-  
15 613, doi.10.1038/nature04668, 2006

16 Sluijs, A., Zachos, J. C., and Zeebe, R. E.: Constraints on hyperthermals, *Nat. Geosci.*, 5, 231-231, doi.10.1038/ngeo1423,  
17 2012

18 Smith, M. E., Carroll, A. R., Scott, J. J., and Singer, B. S.: Early Eocene carbon isotope excursions and landscape  
19 destabilization at eccentricity minima: Green River Formation of Wyoming, *Earth Planet. Sc. Lett.*, 403, 393-406,  
20 doi.10.1016/j.epsl.2014.06.024, 2014

21 Thomas, D. J., Zachos, J. C., Bralower, T. J., Thomas, E., and Bohaty, S.: Warming the fuel for the fire: Evidence for the  
22 thermal dissociation of methane hydrate during the Paleocene-Eocene thermal maximum, *Geology*, 30, 1067-1070, 2002

23 Trenberth, K. E., Hurrell, J. W., and Stepaniak, D. P.: The Asian monsoon: Global perspectives. In: *The Asian Monsoon*,  
24 Wang, B. (Ed.), Springer, New York, 2006.

25 Wang, B. and Fan, Z.: Choice of South Asian summer monsoon indices, *B. Am. Meteorol. Soc.*, 80, 629, 1999

26 Weber, S. L.: The utility of Earth system Models of Intermediate Complexity (EMICs), *Wiley Interdisciplinary Reviews:  
27 Climate Change*, 1, 243-252, doi.10.1002/wcc.24, 2010

28 Westerhold, T., Röhl, U., and Laskar, J.: Time scale controversy: Accurate orbital calibration of the early Paleogene,  
29 *Geochem. Geophys. Geosy.*, 13, doi.10.1029/2012GC004096, 2012

30 Westerhold, T., Röhl, U., McCarren, H. K., and Zachos, J. C.: Latest on the absolute age of the Paleocene–Eocene Thermal  
31 Maximum (PETM): new insights from exact stratigraphic position of key ash layers+ 19 and– 17, *Earth Planet. Sc. Lett.*,  
32 287, 412-419, doi.10.1016/j.epsl.2009.08.027, 2009

33 Williamson, M. S., Lenton, T. M., Shepherd, J. G., and Edwards, N. R.: An efficient numerical terrestrial scheme (ENTS) for  
34 Earth system modelling, *Ecol. Model.*, 198, 362-374, doi.10.1016/j.ecolmodel.2006.05.027, 2006

- 1 Wing, S. L. and Greenwood, D. R.: Fossils and fossil climate: the case for equable continental interiors in the Eocene,  
2 *Philos. T. R. Soc.-B*, 341, 243-252, 1993
- 3 Wyss, G. D. and Jorgensen, K. H.: A User's Guide to LHS: Sandia's Latin Hypercube Sampling Software. Sandia National  
4 Laboratories, Albuquerque, NM, 1998.
- 5 Zachos, J. C., Bohaty, S. M., John, C. M., McCarren, H., Kelly, D. C., and Nielsen, T.: The Palaeocene–Eocene carbon  
6 isotope excursion: constraints from individual shell planktonic foraminifer records, *Philos. T. R. Soc.-A*, 365, 1829-1842,  
7 doi.10.1098/rsta.2007.2045, 2007
- 8 Zachos, J. C., Röhl, U., Schellenberg, S. A., Sluijs, A., Hodell, D. A., Kelly, D. C., Thomas, E., Nicolo, M., Raffi, I.,  
9 Lourens, L. J., McCarren, H., and Kroon, D.: Rapid Acidification of the Ocean during the Paleocene-Eocene Thermal  
10 Maximum, *Science*, 308, 1611-1615, doi.10.2307/3841617, 2005
- 11 Zachos, J. C., Wara, M. W., Bohaty, S., Delaney, M. L., Petrizzo, M. R., Brill, A., Bralower, T. J., and Premoli-Silva, I.: A  
12 transient rise in tropical sea surface temperature during the Paleocene-Eocene thermal maximum, *Science*, 302, 1551-1554,  
13 2003
- 14 Zeebe, R. E., Ridgwell, A., and Zachos, J. C.: Anthropogenic carbon release rate unprecedented during the past 66 million  
15 years, *Nat. Geosci.*, 9, 325–329, doi.10.1038/ngeo2681, 2016
- 16 Zeebe, R. E. and Zachos, J. C.: Long-term legacy of massive carbon input to the Earth system: Anthropocene versus Eocene,  
17 *Philos. T. R. Soc.-A*, 371, 20120006, doi.10.1098/rsta.2012.0006, 2013

18  
19  
20  
21

1 **Table 1** Uniform ranges for forcing and dummy parameters

	min	max
<b>pCO<sub>2</sub> (ppm)</b>	280	3000
<b>Precession (°)</b>	0	360
<b>Obliquity (°)</b>	22.0	24.5
<b>Eccentricity (-)</b>	0.00	0.06
<b>Dummy (-)</b>	0	1

2

3 [Table 2 Forcing factors and dummy values for each member in the ensemble. Precession =  \$\omega\$ , the angle between the](#)  
 4 [moving vernal equinox and the longitude of perihelion.](#)

<a href="#">Member (-)</a>	<a href="#">CO<sub>2</sub> (ppm)</a>	<a href="#">Eccentricity (-)</a>	<a href="#">Precession (°)</a>	<a href="#">Obliquity (°)</a>	<a href="#">Dummy (-)</a>
<a href="#">1</a>	<a href="#">975.6</a>	<a href="#">0.0022</a>	<a href="#">142.5</a>	<a href="#">22.37</a>	<a href="#">0.822</a>
<a href="#">2</a>	<a href="#">2418.7</a>	<a href="#">0.0256</a>	<a href="#">165.2</a>	<a href="#">23.95</a>	<a href="#">0.907</a>
<a href="#">3</a>	<a href="#">1259.4</a>	<a href="#">0.0007</a>	<a href="#">307.1</a>	<a href="#">23.91</a>	<a href="#">0.323</a>
<a href="#">4</a>	<a href="#">801.3</a>	<a href="#">0.0163</a>	<a href="#">270.4</a>	<a href="#">23.50</a>	<a href="#">0.276</a>
<a href="#">5</a>	<a href="#">1720.1</a>	<a href="#">0.0559</a>	<a href="#">206.7</a>	<a href="#">23.82</a>	<a href="#">0.402</a>
<a href="#">6</a>	<a href="#">327.1</a>	<a href="#">0.0595</a>	<a href="#">135.9</a>	<a href="#">23.53</a>	<a href="#">0.681</a>
<a href="#">7</a>	<a href="#">2937.7</a>	<a href="#">0.0418</a>	<a href="#">287.1</a>	<a href="#">22.53</a>	<a href="#">0.650</a>
<a href="#">8</a>	<a href="#">1200.3</a>	<a href="#">0.0237</a>	<a href="#">313.2</a>	<a href="#">24.12</a>	<a href="#">0.978</a>
<a href="#">9</a>	<a href="#">1420.7</a>	<a href="#">0.0158</a>	<a href="#">297.1</a>	<a href="#">23.86</a>	<a href="#">0.931</a>
<a href="#">10</a>	<a href="#">2157.6</a>	<a href="#">0.0432</a>	<a href="#">100.6</a>	<a href="#">23.74</a>	<a href="#">0.661</a>
<a href="#">11</a>	<a href="#">1791.7</a>	<a href="#">0.0241</a>	<a href="#">247.2</a>	<a href="#">23.43</a>	<a href="#">0.429</a>
<a href="#">12</a>	<a href="#">2369.0</a>	<a href="#">0.0425</a>	<a href="#">78.9</a>	<a href="#">22.65</a>	<a href="#">0.167</a>
<a href="#">13</a>	<a href="#">2502.9</a>	<a href="#">0.0296</a>	<a href="#">0.5</a>	<a href="#">22.69</a>	<a href="#">0.122</a>
<a href="#">14</a>	<a href="#">2149.2</a>	<a href="#">0.0405</a>	<a href="#">249.9</a>	<a href="#">24.23</a>	<a href="#">0.347</a>
<a href="#">15</a>	<a href="#">1061.7</a>	<a href="#">0.0394</a>	<a href="#">40.9</a>	<a href="#">23.94</a>	<a href="#">0.189</a>
<a href="#">16</a>	<a href="#">711.3</a>	<a href="#">0.0199</a>	<a href="#">274.6</a>	<a href="#">22.08</a>	<a href="#">0.913</a>
<a href="#">17</a>	<a href="#">1817.1</a>	<a href="#">0.0578</a>	<a href="#">291.4</a>	<a href="#">23.08</a>	<a href="#">0.888</a>
<a href="#">18</a>	<a href="#">722.1</a>	<a href="#">0.0463</a>	<a href="#">195.8</a>	<a href="#">24.38</a>	<a href="#">0.865</a>
<a href="#">19</a>	<a href="#">2988.5</a>	<a href="#">0.0039</a>	<a href="#">110.1</a>	<a href="#">24.40</a>	<a href="#">0.049</a>
<a href="#">20</a>	<a href="#">539.4</a>	<a href="#">0.0251</a>	<a href="#">212.5</a>	<a href="#">23.29</a>	<a href="#">0.234</a>
<a href="#">21</a>	<a href="#">450.6</a>	<a href="#">0.0335</a>	<a href="#">96.1</a>	<a href="#">22.28</a>	<a href="#">0.674</a>
<a href="#">22</a>	<a href="#">2700.1</a>	<a href="#">0.0049</a>	<a href="#">165.9</a>	<a href="#">23.66</a>	<a href="#">0.630</a>
<a href="#">23</a>	<a href="#">2025.4</a>	<a href="#">0.0320</a>	<a href="#">189.4</a>	<a href="#">23.63</a>	<a href="#">0.087</a>
<a href="#">24</a>	<a href="#">2268.7</a>	<a href="#">0.0308</a>	<a href="#">233.3</a>	<a href="#">22.86</a>	<a href="#">0.461</a>
<a href="#">25</a>	<a href="#">1447.2</a>	<a href="#">0.0364</a>	<a href="#">62.0</a>	<a href="#">23.40</a>	<a href="#">0.541</a>
<a href="#">26</a>	<a href="#">1168.3</a>	<a href="#">0.0300</a>	<a href="#">147.4</a>	<a href="#">22.97</a>	<a href="#">0.947</a>
<a href="#">27</a>	<a href="#">1317.6</a>	<a href="#">0.0377</a>	<a href="#">12.4</a>	<a href="#">23.04</a>	<a href="#">0.714</a>
<a href="#">28</a>	<a href="#">1639.5</a>	<a href="#">0.0265</a>	<a href="#">150.9</a>	<a href="#">22.98</a>	<a href="#">0.524</a>
<a href="#">29</a>	<a href="#">399.0</a>	<a href="#">0.0589</a>	<a href="#">262.7</a>	<a href="#">23.46</a>	<a href="#">0.028</a>
<a href="#">30</a>	<a href="#">2876.3</a>	<a href="#">0.0411</a>	<a href="#">203.0</a>	<a href="#">22.05</a>	<a href="#">0.608</a>
<a href="#">31</a>	<a href="#">2611.1</a>	<a href="#">0.0170</a>	<a href="#">54.3</a>	<a href="#">22.84</a>	<a href="#">0.746</a>
<a href="#">32</a>	<a href="#">2831.7</a>	<a href="#">0.0564</a>	<a href="#">187.2</a>	<a href="#">23.72</a>	<a href="#">0.696</a>
<a href="#">33</a>	<a href="#">1998.5</a>	<a href="#">0.0372</a>	<a href="#">278.8</a>	<a href="#">24.19</a>	<a href="#">0.805</a>

<a href="#">34</a>	<a href="#">1465.0</a>	<a href="#">0.0439</a>	<a href="#">38.9</a>	<a href="#">23.50</a>	<a href="#">0.376</a>
<a href="#">35</a>	<a href="#">1660.0</a>	<a href="#">0.0109</a>	<a href="#">85.3</a>	<a href="#">22.88</a>	<a href="#">0.896</a>
<a href="#">36</a>	<a href="#">2393.7</a>	<a href="#">0.0587</a>	<a href="#">127.9</a>	<a href="#">24.27</a>	<a href="#">0.191</a>
<a href="#">37</a>	<a href="#">286.3</a>	<a href="#">0.0004</a>	<a href="#">27.1</a>	<a href="#">23.99</a>	<a href="#">0.391</a>
<a href="#">38</a>	<a href="#">667.4</a>	<a href="#">0.0509</a>	<a href="#">116.5</a>	<a href="#">22.71</a>	<a href="#">0.569</a>
<a href="#">39</a>	<a href="#">2246.8</a>	<a href="#">0.0450</a>	<a href="#">317.4</a>	<a href="#">22.90</a>	<a href="#">0.103</a>
<a href="#">40</a>	<a href="#">2334.2</a>	<a href="#">0.0096</a>	<a href="#">294.7</a>	<a href="#">23.61</a>	<a href="#">0.532</a>
<a href="#">41</a>	<a href="#">2968.2</a>	<a href="#">0.0346</a>	<a href="#">329.8</a>	<a href="#">22.51</a>	<a href="#">0.314</a>
<a href="#">42</a>	<a href="#">768.2</a>	<a href="#">0.0085</a>	<a href="#">218.3</a>	<a href="#">23.00</a>	<a href="#">0.000</a>
<a href="#">43</a>	<a href="#">925.8</a>	<a href="#">0.0450</a>	<a href="#">327.2</a>	<a href="#">24.32</a>	<a href="#">0.753</a>
<a href="#">44</a>	<a href="#">384.5</a>	<a href="#">0.0081</a>	<a href="#">60.6</a>	<a href="#">22.59</a>	<a href="#">0.436</a>
<a href="#">45</a>	<a href="#">850.7</a>	<a href="#">0.0551</a>	<a href="#">322.9</a>	<a href="#">23.21</a>	<a href="#">0.459</a>
<a href="#">46</a>	<a href="#">1112.8</a>	<a href="#">0.0150</a>	<a href="#">356.7</a>	<a href="#">23.27</a>	<a href="#">0.579</a>
<a href="#">47</a>	<a href="#">1255.8</a>	<a href="#">0.0116</a>	<a href="#">212.2</a>	<a href="#">22.31</a>	<a href="#">0.487</a>
<a href="#">48</a>	<a href="#">1124.1</a>	<a href="#">0.0530</a>	<a href="#">343.7</a>	<a href="#">22.40</a>	<a href="#">0.065</a>
<a href="#">49</a>	<a href="#">2113.9</a>	<a href="#">0.0276</a>	<a href="#">9.9</a>	<a href="#">22.19</a>	<a href="#">0.856</a>
<a href="#">50</a>	<a href="#">1681.0</a>	<a href="#">0.0354</a>	<a href="#">175.5</a>	<a href="#">22.45</a>	<a href="#">0.287</a>

1

2

3 **Table 32** R<sup>2</sup> correlation between PC scores from SVD and PC scores emulated with the linear models.

	<b>PC1</b>	<b>PC2</b>	<b>PC3</b>
<b>DJF_temperature</b>	0.95	0.58	0.75
<b>JJA_temperature</b>	0.97	0.97	0.72
<b>DJF_precipitation</b>	0.97	0.92	0.64
<b>JJA_precipitation</b>	0.99	0.99	0.89

4

5

6 **Table 43** Total effects of forcing parameters on simple scalar metrics.

	<b>CO<sub>2</sub></b>	<b>Eccentricity</b>	<b>Obliquity</b>	<b>Precession</b>
<b>MAT</b>	0.996	0.002	0.000	0.002
<b>N_seasonality</b>	0.873	0.025	0.013	0.088
<b>N_winter TPTD</b>	0.974	0.009	0.010	0.007
<b>N_summer TPTD</b>	0.084	0.046	0.640	0.229
<b>S_winter POLC</b>	0.996	0.000	0.000	0.004
<b>N_winter POLC</b>	0.268	0.018	0.659	0.055
<b>Asian monsoon index</b>	0.087	0.078	0.073	0.762
<b>African monsoon index</b>	0.061	0.137	0.010	0.792

7

8

9

	<u>CO<sub>2</sub></u>	<u>Eccentricity</u>	<u>Obliquity</u>	<u>Precession</u>
<u>MAT</u>	<u>0.993</u>	<u>0.002</u>	<u>0.000</u>	<u>0.005</u>
<u>N. seasonality</u>	<u>0.766</u>	<u>0.003</u>	<u>0.011</u>	<u>0.220</u>
<u>N. winter TPTD</u>	<u>0.939</u>	<u>0.006</u>	<u>0.039</u>	<u>0.017</u>
<u>N. summer TPTD</u>	<u>0.144</u>	<u>0.000</u>	<u>0.673</u>	<u>0.183</u>
<u>S. winter POLC</u>	<u>0.979</u>	<u>0.004</u>	<u>0.005</u>	<u>0.012</u>
<u>N. winter POLC</u>	<u>0.088</u>	<u>0.000</u>	<u>0.789</u>	<u>0.122</u>
<u>Asian monsoon index</u>	<u>0.094</u>	<u>0.004</u>	<u>0.063</u>	<u>0.840</u>
<u>African monsoon index</u>	<u>0.017</u>	<u>0.001</u>	<u>0.001</u>	<u>0.981</u>
<u>American monsoon index</u>	<u>0.490</u>	<u>0.004</u>	<u>0.020</u>	<u>0.486</u>

1 Table 54 R<sup>2</sup> correlation values for PC scores for temperature and precipitation in DJF and JJA. Values where R<sup>2</sup> >= 0.5  
 2 are shown in red.

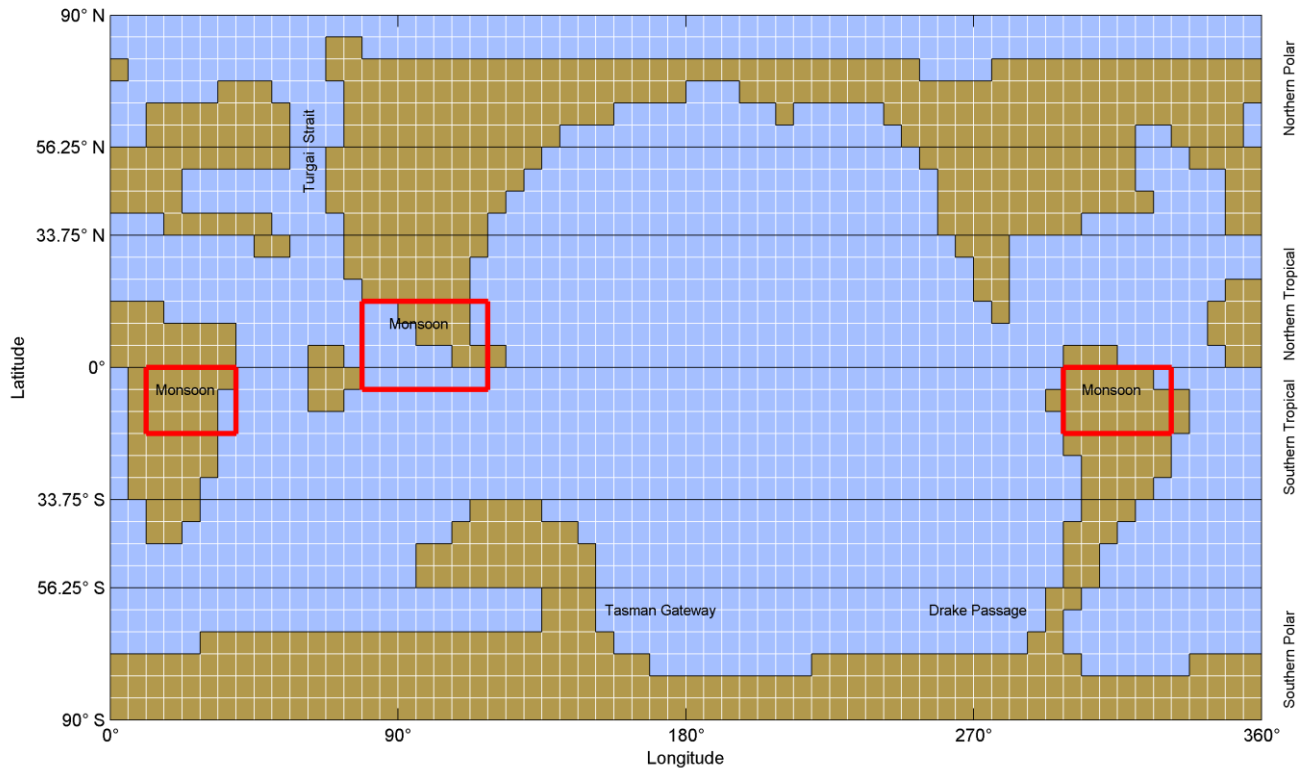
		DJF_precipitation		
		PC1	PC2	PC3
DJF_temperature	PC1	<b>0.993</b>	-0.004	-0.080
	PC2	-0.067	-0.364	<b>-0.864</b>
	PC3	0.005	<b>0.783</b>	-0.354
		JJA_precipitation		
		PC1	PC2	PC3
JJA_temperature	PC1	<b>0.976</b>	0.091	0.157
	PC2	0.098	<b>-0.947</b>	0.082
	PC3	-0.180	-0.049	<b>0.795</b>

3

4

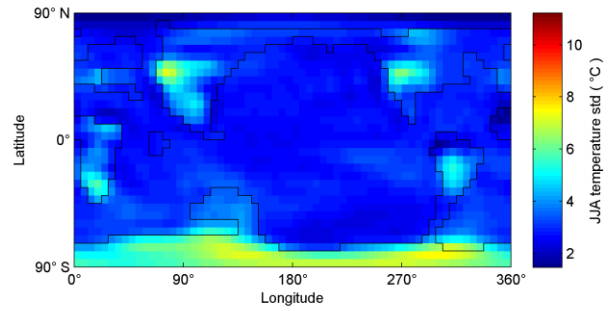
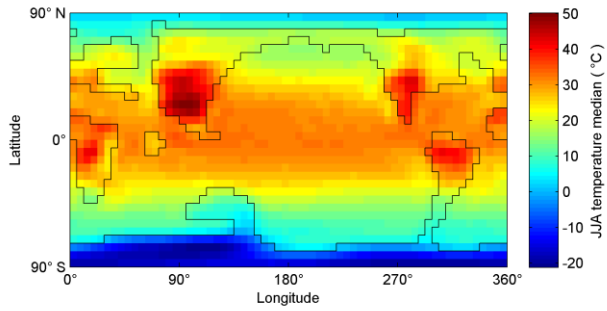
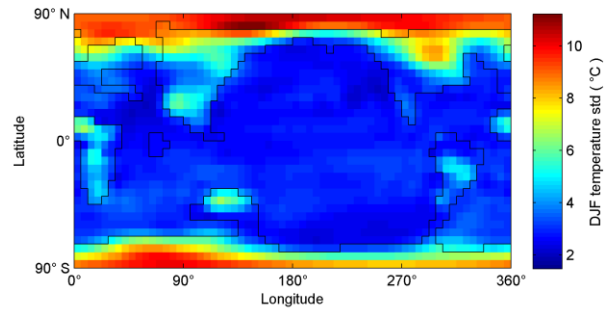
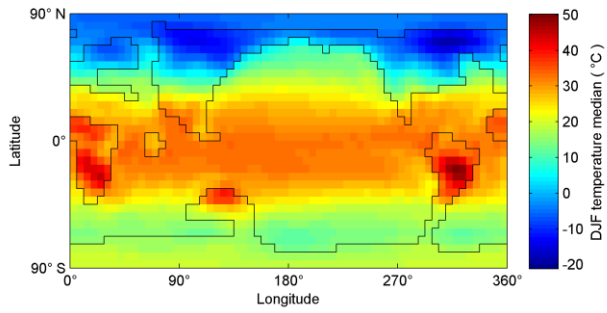
5 Table 65 R<sup>2</sup> correlation values for forcing factors and PC scores. Values where R<sup>2</sup> >= 0.5 are shown in red.

		precession		
		CO <sub>2</sub>	index	obliquity
DJF_temperature	PC1	<b>-0.859</b>	-0.018	-0.057
	PC2	0.381	-0.087	-0.354
	PC3	0.038	<b>-0.924</b>	0.311
JJA_temperature	PC1	<b>-0.899</b>	0.178	-0.066
	PC2	-0.018	<b>-0.875</b>	0.362
	PC3	0.342	0.056	-0.239
DJF_precipitation	PC1	<b>-0.867</b>	0.003	-0.025
	PC2	-0.198	<b>-0.820</b>	0.044
	PC3	-0.278	0.465	0.164
JJA_precipitation	PC1	<b>-0.953</b>	0.065	0.008
	PC2	-0.070	<b>0.960</b>	-0.131
	PC3	0.219	0.191	-0.029



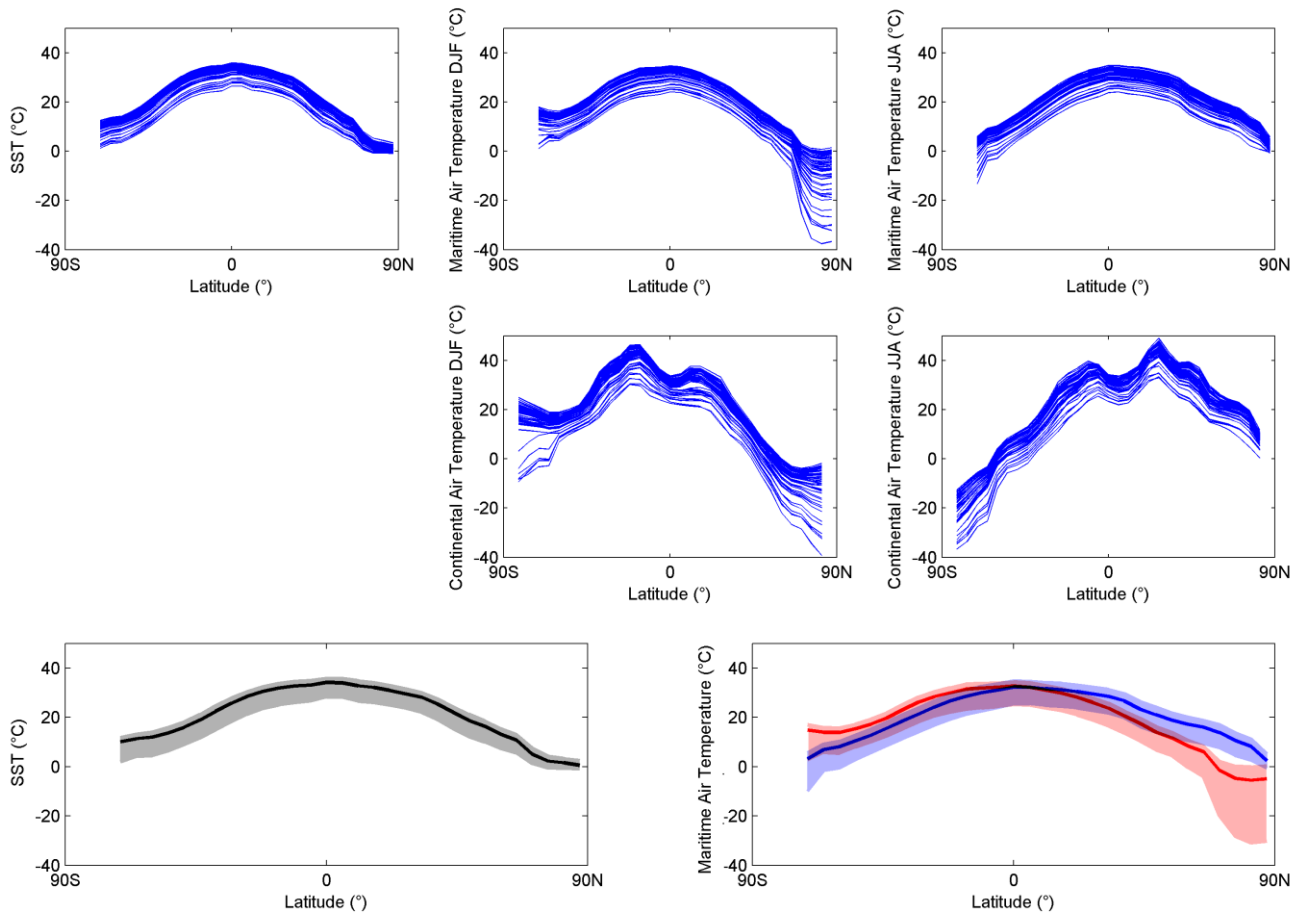
1  
2 **Figure 1: Eocene palaeogeography and geographic areas used to determine simple metric values**

3



1  
2  
3

**Figure 2: Ensemble temperature medians (left column) and standard deviations (right column) in DJF (top row) and JJA (bottom row).**



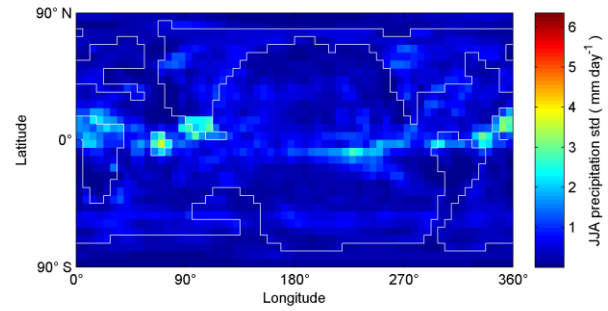
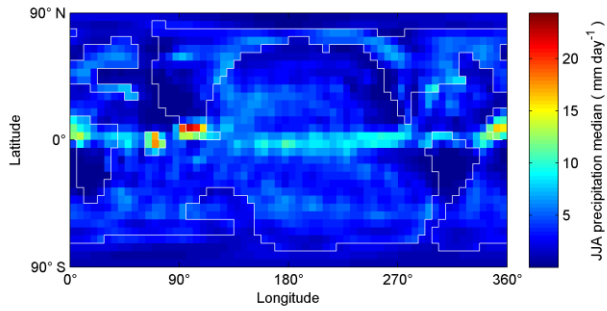
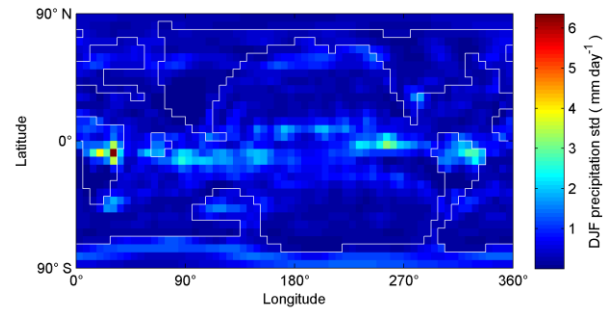
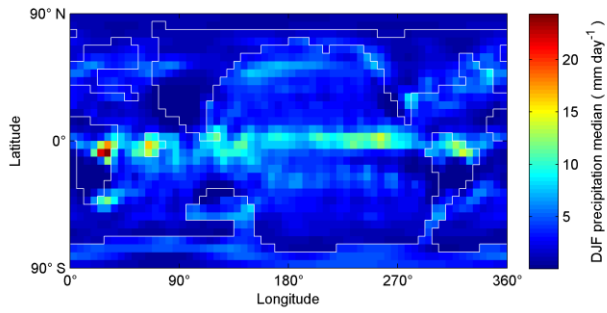
1

2 **Figure 3: Top: full ensemble distributions of mean latitude values of global annual mean sea surface temperature (SST), with**  
 3 **mean latitude maritime surface air temperature in DJF and JJA.**

4 **Middle: mean latitude continental surface air temperature in DJF and JJA.**

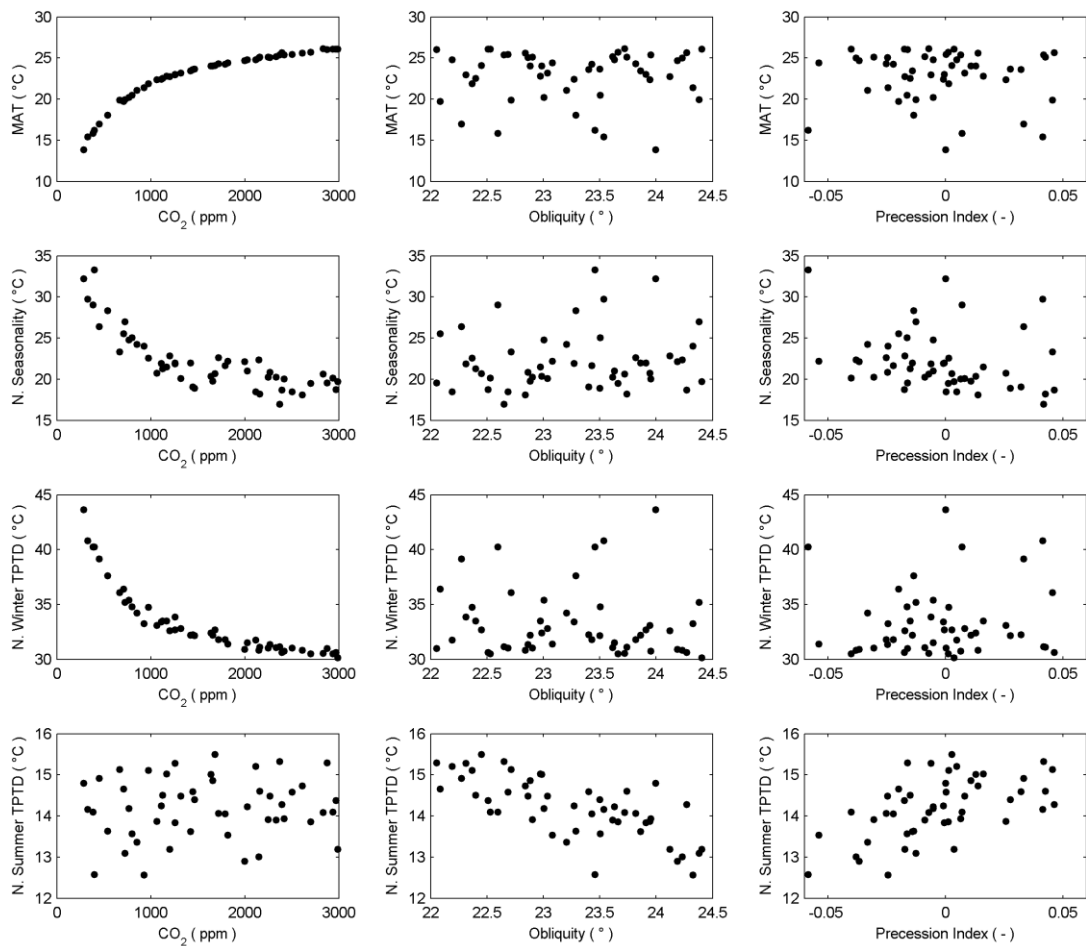
5 **Bottom: ensemble medians and 5% and 95% percentiles of global annual mean SST, and maritime surface air temperature in DJF**  
 6 **(red) and JJA (blue).**

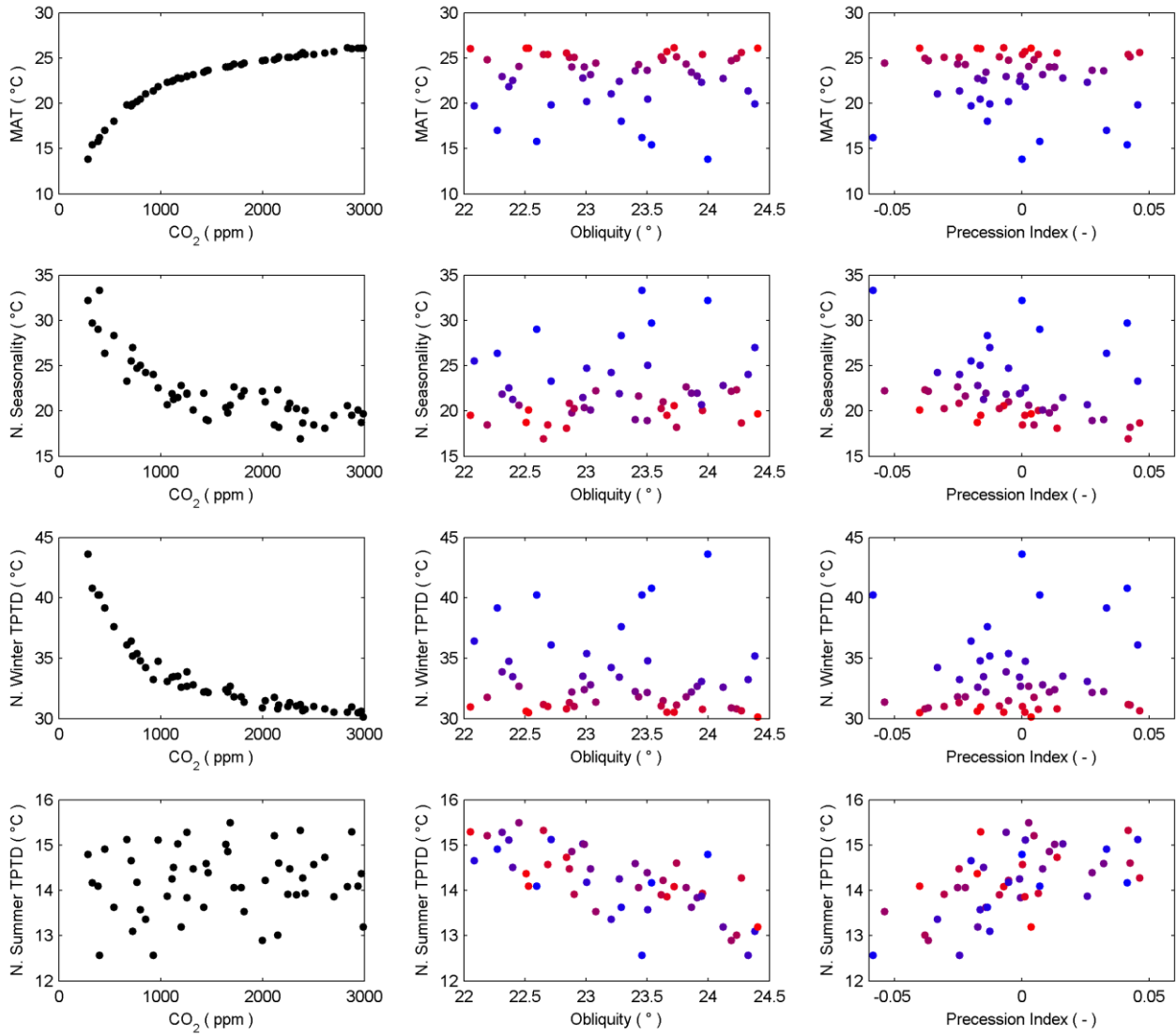
7



1  
2  
3

**Figure 4: Ensemble precipitation medians (left column) and standard deviations (right column) in DJF (top row) and JJA (bottom row).**

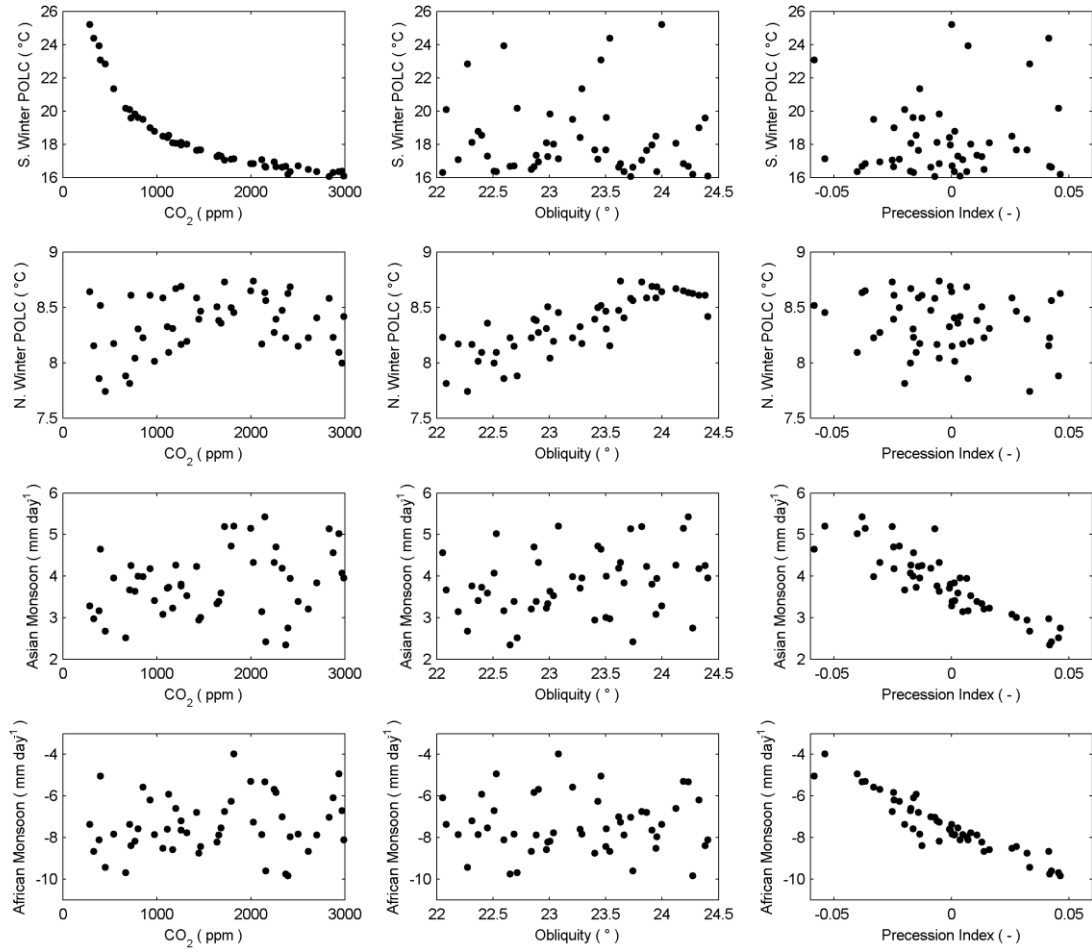


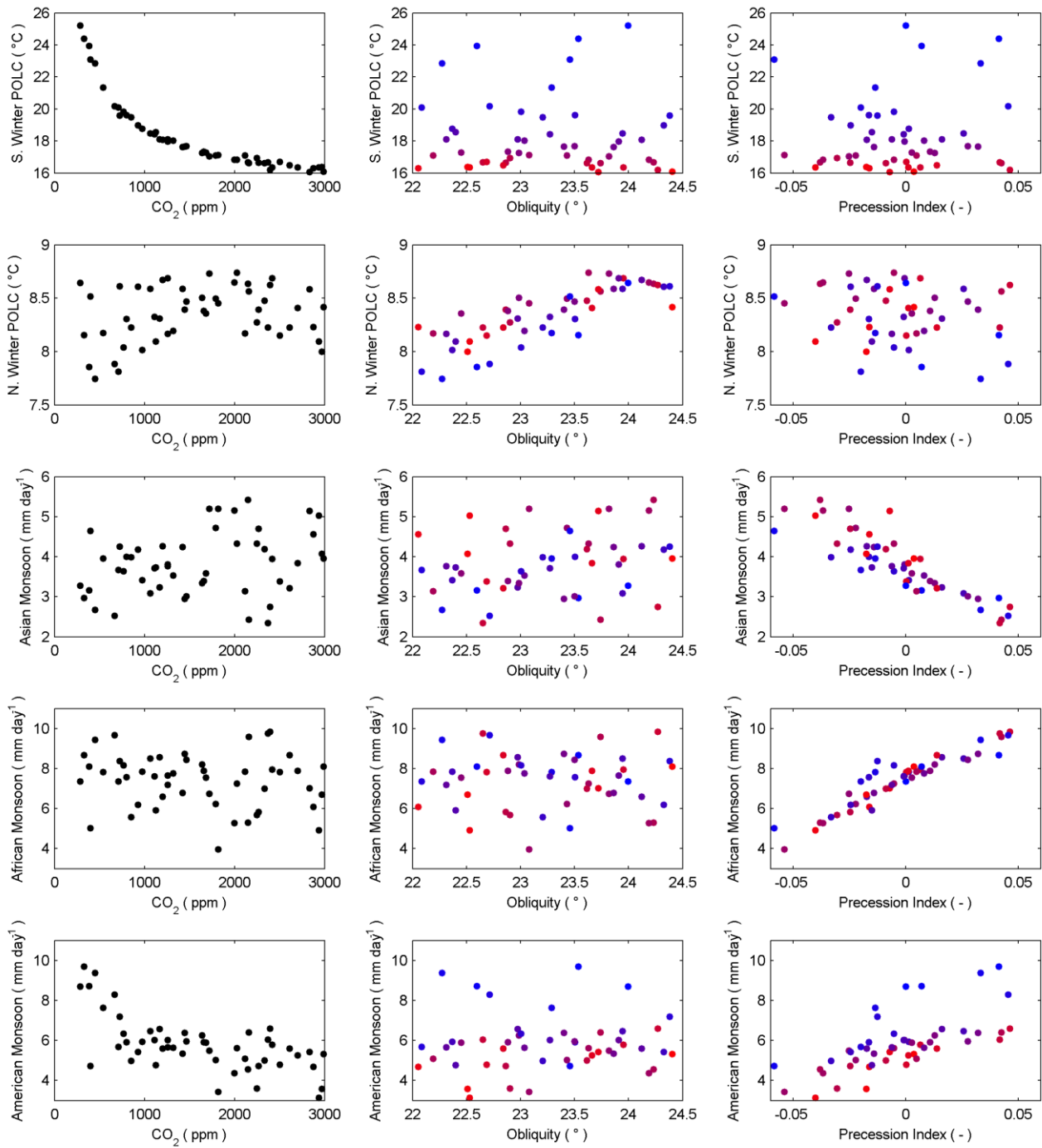


1

2 **Figure 5: Correlation between three forcing factors CO<sub>2</sub>, obliquity and precession index (in columns from left to right), and the**  
 3 **simple metrics MAT, northern seasonality, northern winter tropical-polar temperature difference and northern summer tropical-**  
 4 **polar temperature difference (in rows from top to bottom). CO<sub>2</sub> is plotted in colour in the obliquity and precession plots (blue =**  
 5 **low, red = high)**

6

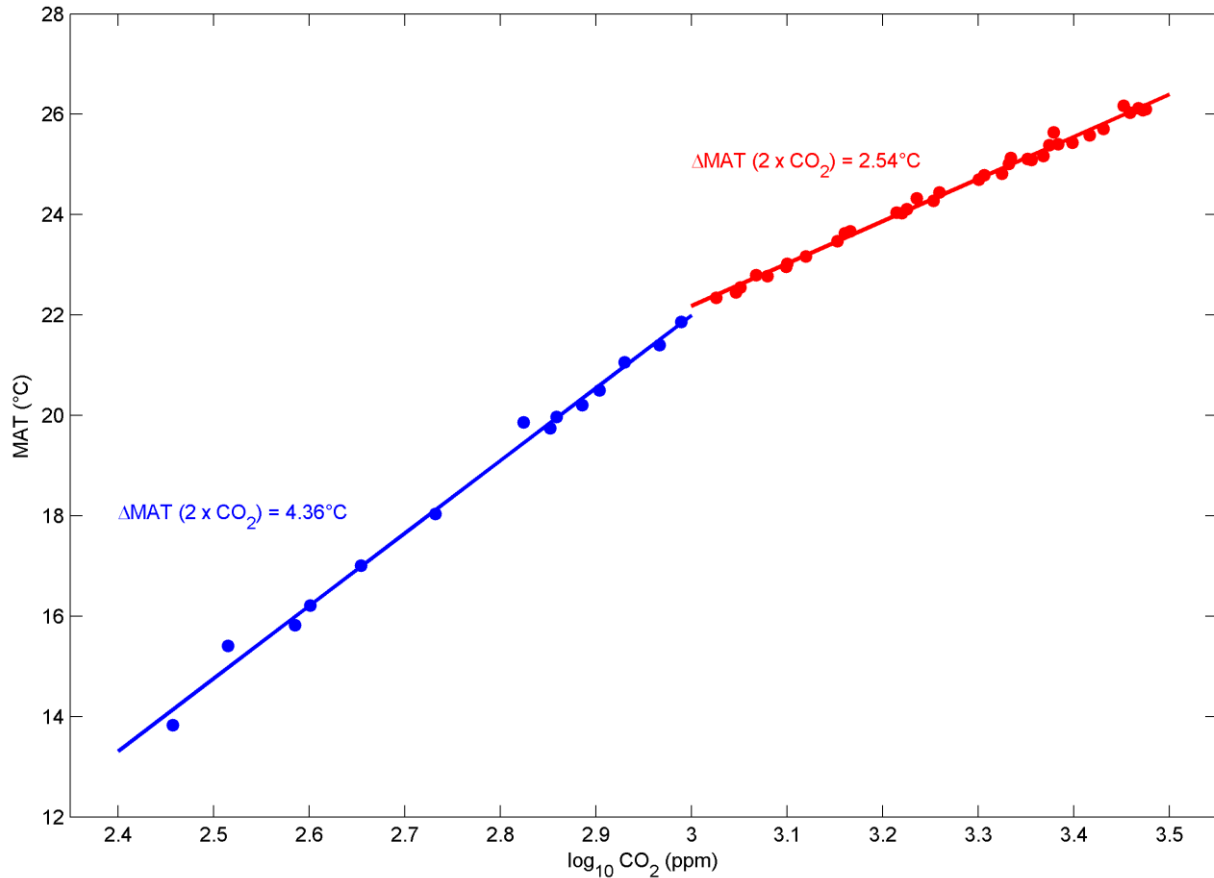




1 **Figure 6: Correlation between three forcing factors CO<sub>2</sub>, obliquity and precession index (in columns from left to right), and the**  
2 **simple metrics southern winter polar OLC, northern winter polar OLC, Asian monsoon index, ~~and~~ African monsoon index and**  
3 **American monsoon index (in rows from top to bottom). CO<sub>2</sub> is plotted in colour in the obliquity and precession plots (blue = low,**  
4 **red = high)**

5

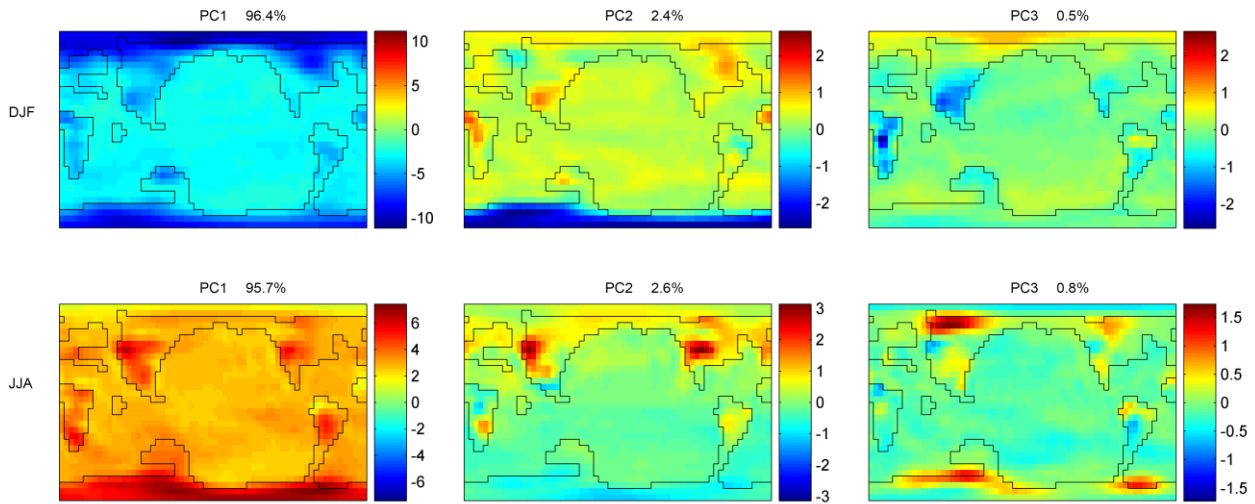
6



7

8 Figure 7: Mean air temperature plotted against CO<sub>2</sub> on a logarithmic scale, with regression lines plotted for CO<sub>2</sub> < 1000 ppm  
9 (blue), and CO<sub>2</sub> > 1000 ppm (red), with climate sensitivities for a doubling of CO<sub>2</sub> from both of the regressions.

1

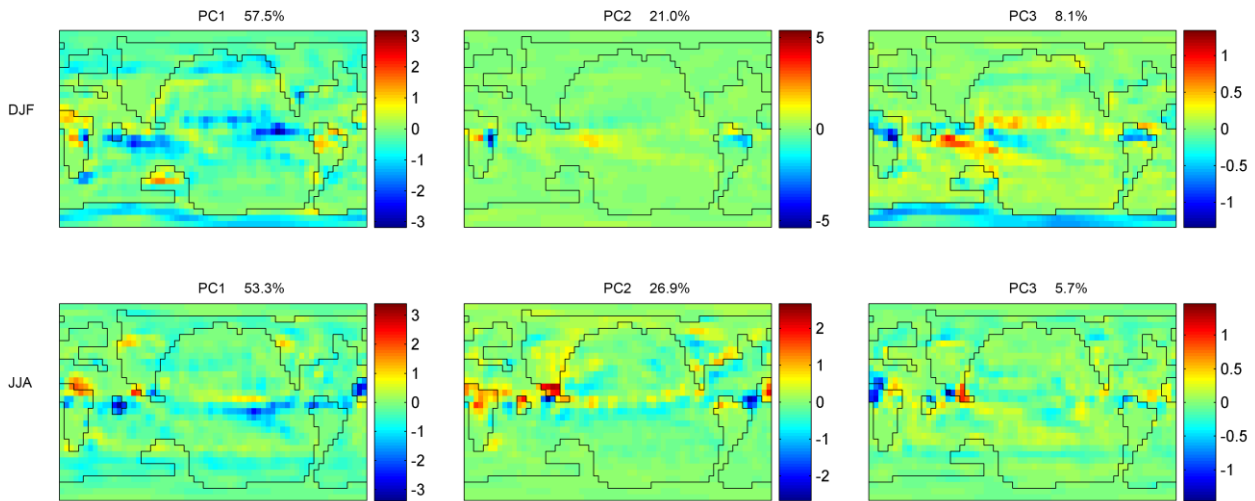


2

3 **Figure 78:** The first three principal components of DJF\_temperature (top row) and JJA\_temperature (bottom row). Percentages  
4 of variance explained by each principal component are shown above each plot.

5

6

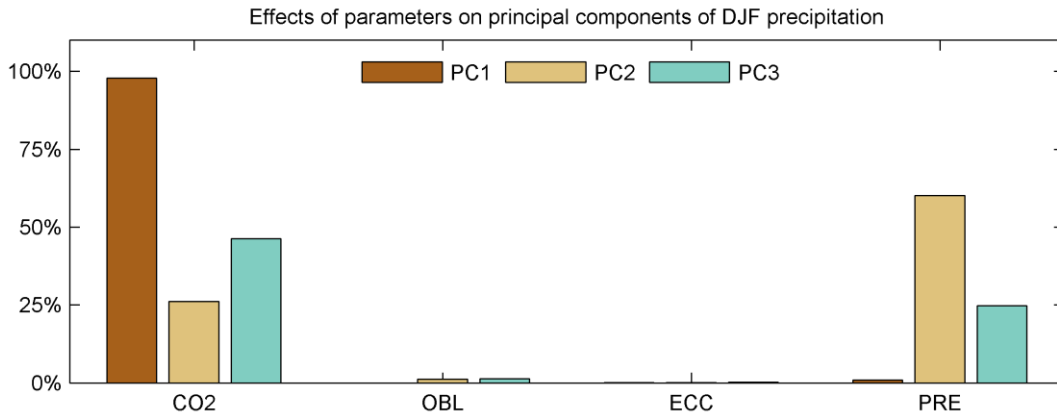
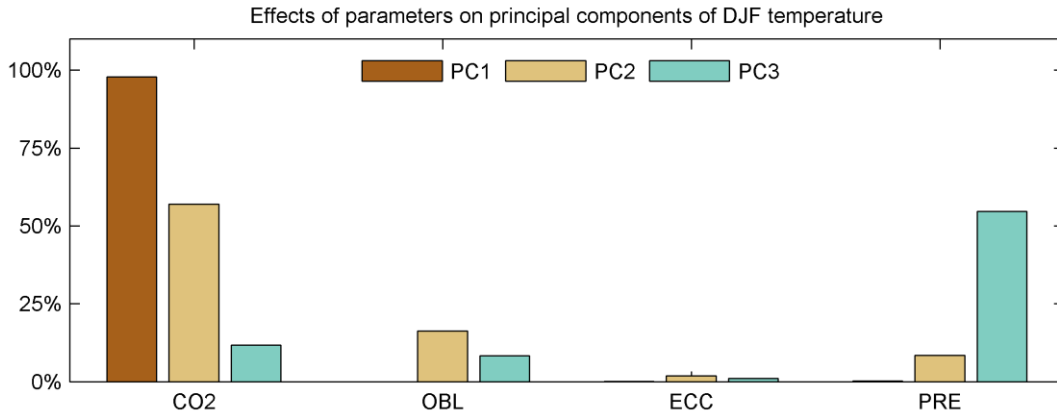


7

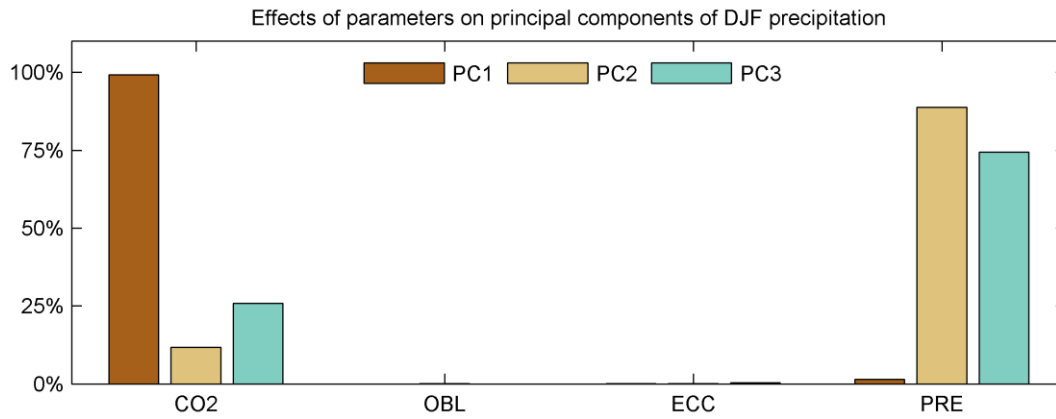
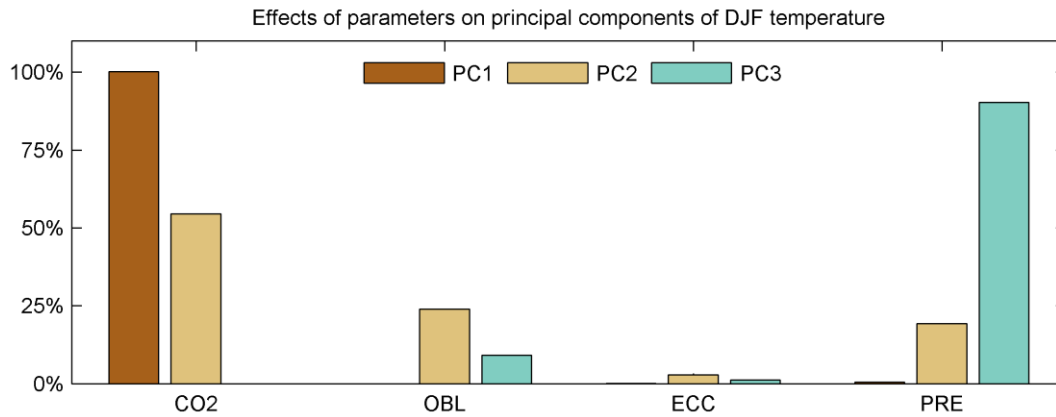
8 **Figure 89:** The first three principal components of DJF\_precipitation (top row) and JJA\_precipitation (bottom row). Percentages  
9 of variance explained by each principal component are shown above each plot.

10

1



2



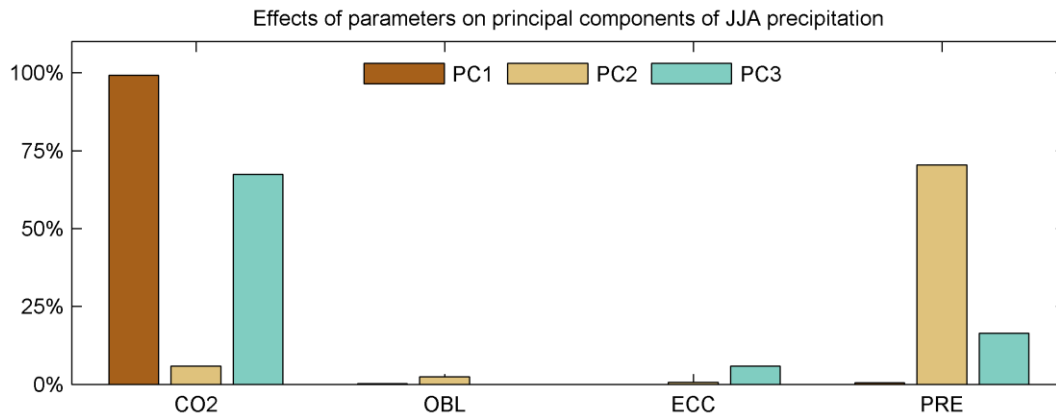
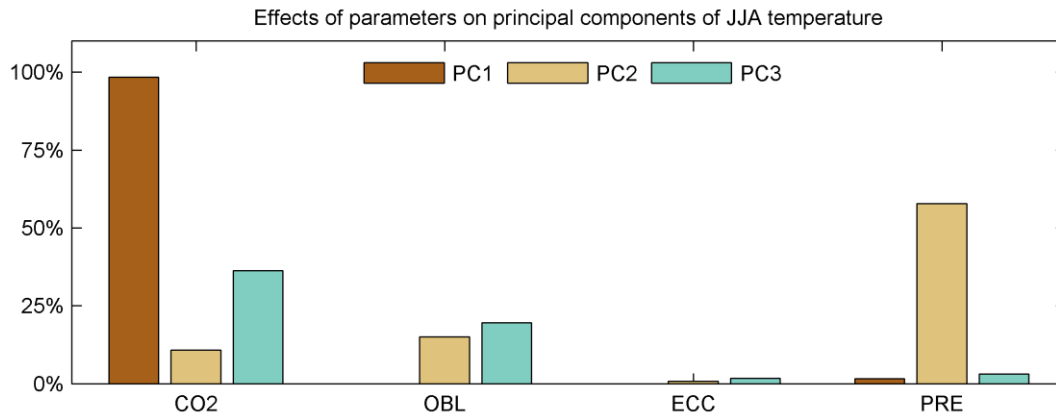
1

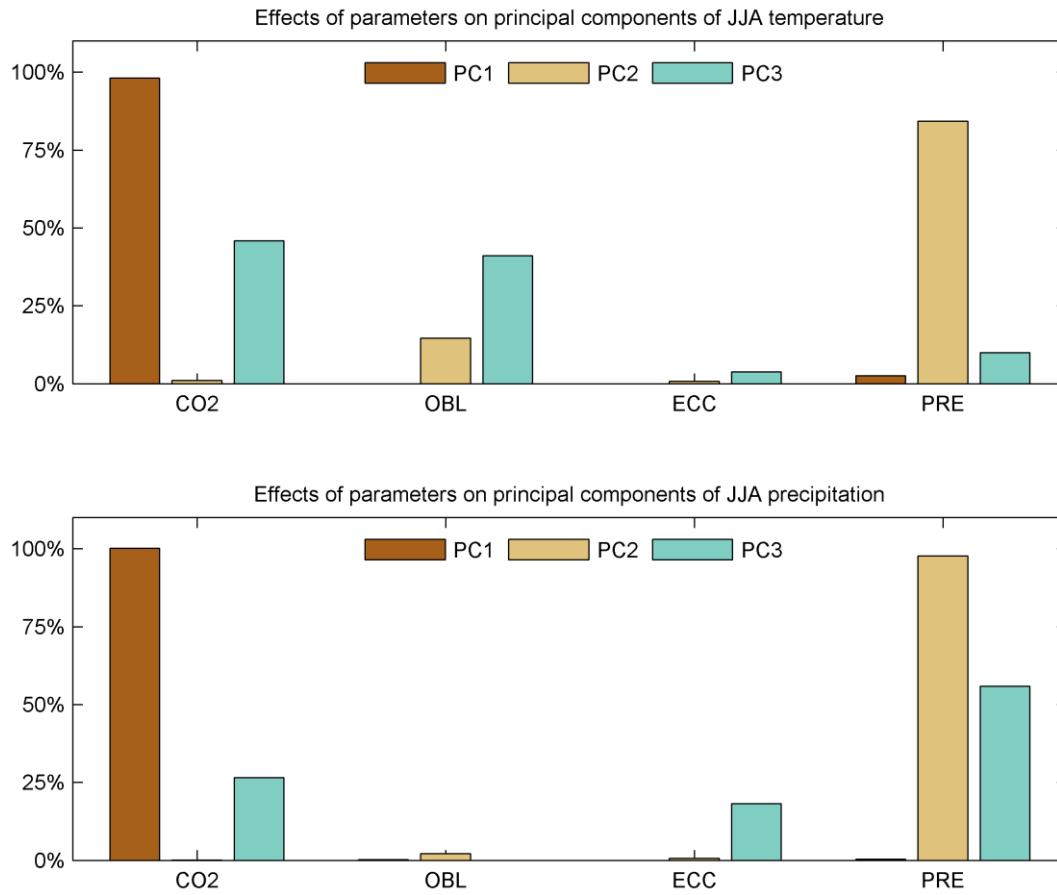
2 **Figure 910: Main effects of forcing parameters on the first three principal components of DJF\_temperature (top row) and**  
 3 **DJF\_precipitation (bottom row).**

4

5

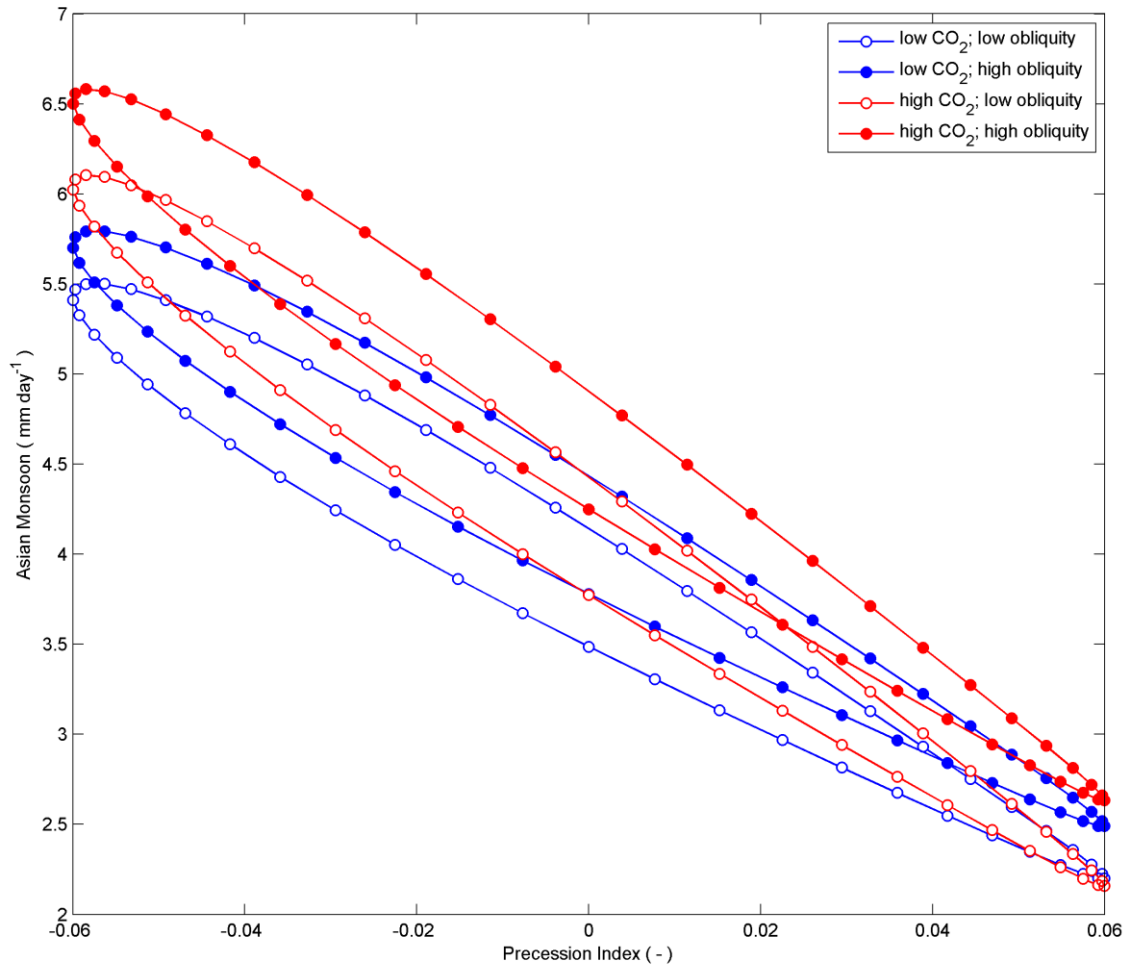
6





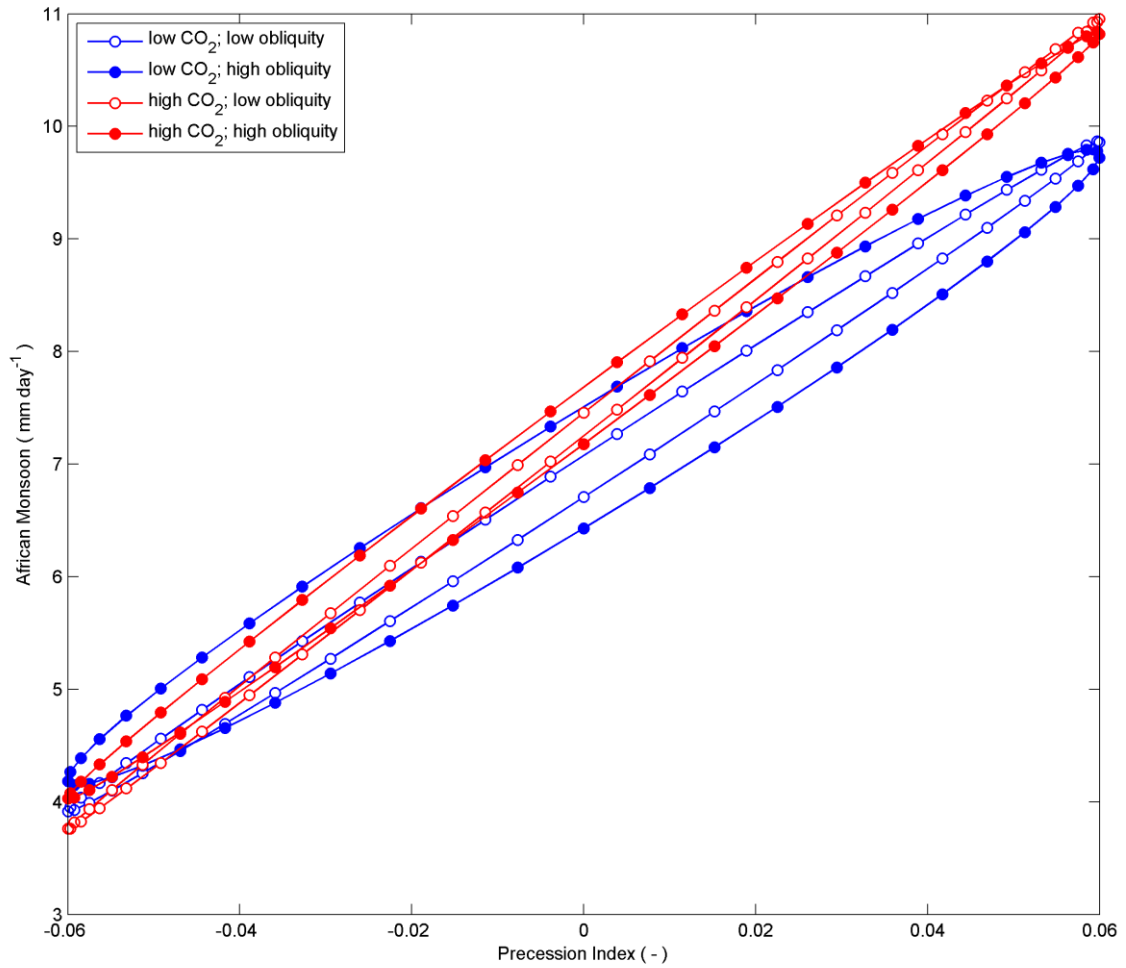
1

2 **Figure 4011:** Main effects of forcing parameters on the first three principal components of JJA\_temperature (top row) and  
 3 JJA\_precipitation (bottom row).



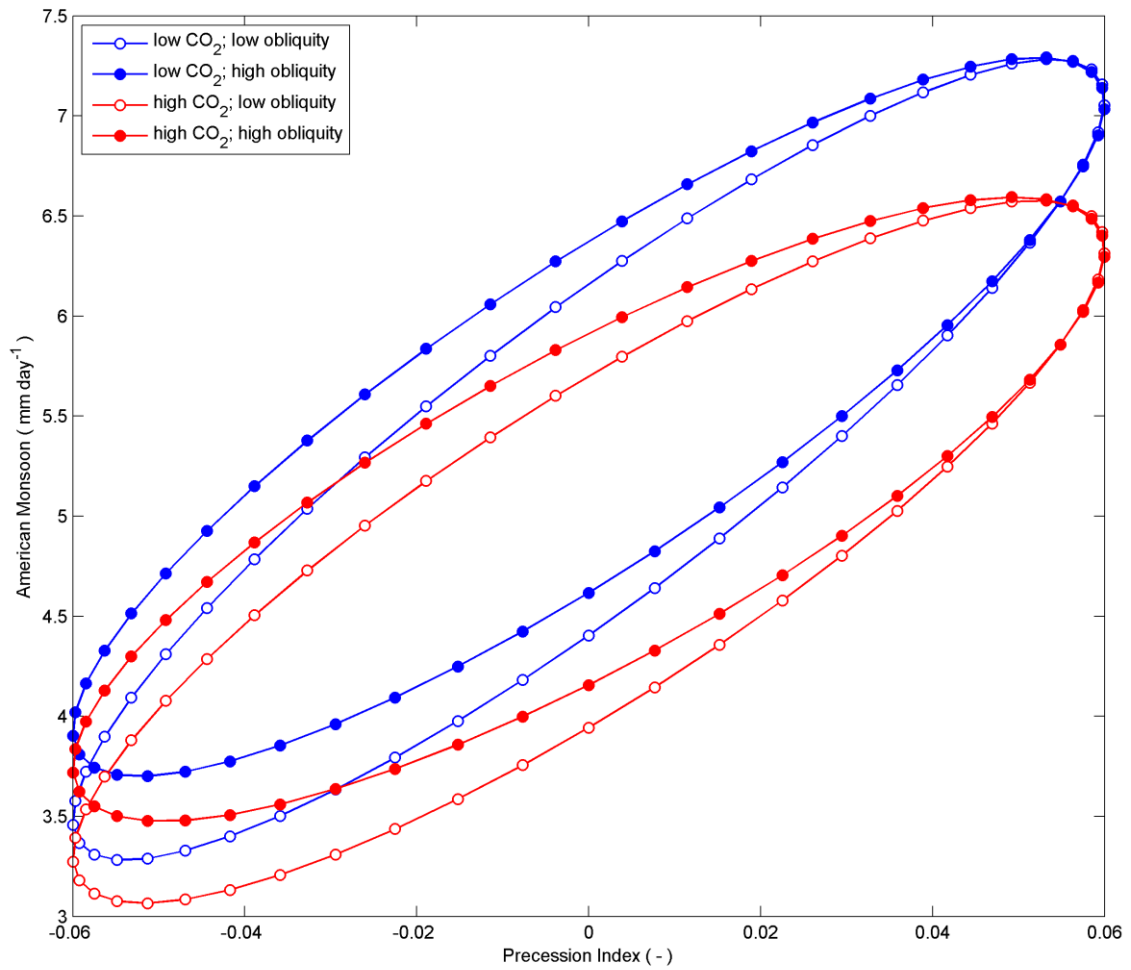
1

2 [Figure 12: Emulated values of the Asian monsoon index, for the full range of the precession index \( \$\epsilon \sin \omega\$ \), at low and high values](#)  
 3 [of CO<sub>2</sub> and obliquity \( \$\epsilon\$ \).](#)



1

2 Figure 13: Emulated values of the African monsoon index, for the full range of the precession index ( $\epsilon \sin \omega$ ), at low and high values  
 3 of CO<sub>2</sub> and obliquity ( $\epsilon$ ).



1

2 [Figure 14: Emulated values of the American monsoon index, for the full range of the precession index \( \$\epsilon \sin \omega\$ \), at low and high](#)  
 3 [values of CO<sub>2</sub> and obliquity \( \$\epsilon\$ \).](#)